8-15-2014 12:00 AM

Dual energy imaging for determining urinary calculi composition: A theoretical and experimental study with computed tomography

Stephanie Nykamp
The University of Western Ontario

Supervisor
Dr. Ian Cunningham
The University of Western Ontario

Graduate Program in Medical Biophysics
A thesis submitted in partial fulfillment of the requirements for the degree in Master of Science

DUAL ENERGY IMAGING FOR DETERMINING URINARY CALCULI COMPOSITION: A THEORETICAL AND EXPERIMANTAL STUDY WITH COMPUTED TOMOGRAPHY

(Thesis format: Integrated Article)

by

Stephanie Nykamp

Graduate Program in Medical Biophysics

A thesis submitted in partial fulfillment
of the requirements for the degree of
Masters of Medical Biophysics

The School of Graduate and Postdoctoral Studies
The University of Western Ontario
London, Ontario, Canada

Abstract

Urinary calculi is a common problem worldwide and is associated with substantial patient morbidity and healthcare costs. The choice of treatment is dependent on the composition of the stone. Currently that can only be determined once it has been removed which is too late to impact treatment decisions. Considerable investigation into the use of dual-energy CT (DECT) for determining stone composition has lead to mixed results. The varied results may be due to inherent sources of error and it is unclear whether the mixed results with DECT are due to CT artifacts or insufficient fundamental difference in the linear attenuation coefficient between stones of various compositions. This work will develop a fundamental model for dual-energy CT to determine the ability to differentiate between stones of uniform and mixed composition. The model will be tested experimentally to optimize the parameters and determine the appropriate clinical measurement to reflect the results.

Keywords: Dual-energy, urinary calculi, CT, composition

Acknowledgments

I would like to thank Ian Cunningham for his unending patience and guidance.

Table of Contents

List of Tables

List of Figures

List of Appendices

Chapter 1 – Introduction and Review of the Literature

1.1 Introduction

Urolithiasis is a common disease that is associated with significant morbidity and a prevalence of 3-20% worldwide.(1, 2) Stones can either form in the bladder or the kidneys. Kidney stones can subsequently move into the ureters where, depending on the size, they will either continue to pass into the urinary bladder or cause obstruction of the ureter causing substantial pain and potential renal dysfunction. Management of urinary stones involves initial diagnosis, removal and prevention of recurrence. Stones can be made of various different mineral compositions and can either relatively hard or soft. Additionally they are of variable densities and may be unapparent on radiographs. CT has become the standard of care in the identification of renal and ureteral stones in people because of the improved sensitivity and specificity compared to plain radiographs (3, 4) but has had variable results in the ability to determine the composition of the stones.(4-17) Once diagnosed, stones in the kidney and proximal ureter can be treated with ureteroscopy, surgery, percutaneous nephrolithotomy or extracorporeal shock wave lithotripsy (ESWL).(18) Extracorporeal shock wave lithotripsy is a preferred treatment because it is minimally invasive but it is not effective for all compositions of stones. Although not specifically contraindicated in hard stones ESWL can result in renal and systemic side effects and incompletely fragment a stone into multiple large pieces that still cannot pass and are more difficult to retrieve with more invasive methods resulting in increased patient morbidity.(19, 20) Therefore, determining stone composition in vivo would be beneficial to treatment planning to reduce patient morbidity.

Plain CT and dual energy CT have been used to determine stone composition with varied results. Inconsistency in the results may be due to the varied study design, including varied imaging parameters and criteria for a pure stone composition, differences in system calibration, scanner specific proprietary filters, beam hardening and partial volume averaging artifact. An example that some studies may be imaging artifact is seen

in Graser et al. in 2008 where a image of a stone composed of two materials is provided.(21) This image illustrates a linear band of material traversing the entire diameter of the stone. Formation of stones typically occurs by deposition of concentric rings around a central nidus. This linear deposition has never been reported and therefore this image may represent detection of an artifact rather than a true difference in stone material. The question remains whether it is fundamentally possible to determine stone composition with dual energy CT.

To address the varying published results on dual energy CT for determining stone composition the fundamental question of whether there is sufficient difference in the dual energy measurement between stones must be evaluated. If there is insufficient difference in the measurement between pure stones then detecting differences in stones of mixed composition with systems that have inherent sources of error will never be effective. This work will evaluate the fundamental signal to noise ratio for common stone materials to determine whether there is sufficient difference to differentiate stone materials. In addition it will assess the utility of task specific beam filtration in improving the difference in signal to noise ratio between stone materials to determine there is improved differentiation. Finally, dual energy CT will be evaluated in an experimental model to determine if it can differentiate common canine stone materials in a phantom.

1.2 Urolithiasis

There is a geographic predisposition to urolithiasis with the highest prevalence's noted in North America, Japan, and Scandinavia.(2) In the past decades there has been a decrease in the prevalence of bladder stones with a concurrent increase in the prevalence of renal stones that is thought to be due to changes in eating habits and a trend to large amount of high protein foods.(2) In addition to this shift in stone origin the overall incidence and prevalence of this disease is increasing worldwide having only peaked in North America in the 1980's and in European and Asian countries in the 1990's and 2000's.(2, 22) Urolithiasis is also a common problem in dogs and cats with an reported incidence of

2.8% of all dogs and 1-10% of all cats.(23) In spite of advances in the understanding of the pathogenesis, urolithiasis remains a common disorder.

An understanding of stone composition and how it influences treatment options is required to appreciate the challenges and importance of in vivo diagnosis.

1.2.1 Diagnosis of urolithiasis

The goals of initial imaging tests in the diagnosis of urolithiasis are (1) accurately determine the presence of stones, (2) determine the size of the stone, and (3) determine the composition of the stone. Size and composition are important factors in deciding on the appropriate treatment for uroliths. For example, uric acid stones are amenable to medical management (by alkalization of the urine) and ESWL while calcium oxalate stones cannot be treated medically and are less likely to be completely fragmented by ESWL so percutaneous nephrolithotomy may required for definitive treatment.(8) Stones of greater than 2 cm in diameter are typically not treated with ESWL as they are difficult to fragment sufficiently to pass through the ureter without causing obstruction.(14)

Plain radiographs have been evaluated for their ability to predict the composition of renal stones. Evaluation can be subjective by assessing shape, architecture, and comparing stone density to a rib or vertebrae or objective through grey scale analysis.(24, 25) The disadvantage of plain radiographs is that stones must be of a minimum size and calcium content to be detected due to the superimposition of soft tissue structures and bowel gas. Urate and cystine stones typically have insufficient density to be detected on plain radiographs. Levine et. al showed that 41-55% of ureteral stones evident on CT were not evident on plain radiographs regardless of composition.(3) Although subjective assessment of stone composition is highly inaccurate, Oehlschlager et. al. showed that grey scale analysis of scanned films differentiated between calcium oxalate stones and magnesium ammonium phosphate (MAP)/calcium phosphate stones in 100% of cases but could not differentiate between MAP and calcium phosphate stones.(24, 25) Stone radiodensity has also been compared to the 12^{th} rib but could not predict the stone composition or the efficacy of ESWL.(26)

As previously discussed, CT has become the standard of care in the identification of renal and ureteral stones in people because of the improved sensitivity and specificity compared to plain radiographs.(3, 4) An additional advantage is the ability to detect extra urinary causes of flank pain that can mimic ureteral colic. Because CT is often already being performed in this patient population and it has the ability to quantitate the density of materials there has been considerable interest in the use of single and dual energy CT for determining stone composition in vitro to facilitate treatment decisions.

1.2.2 Composition of calculi

Calculi are described in terms of their mineral composition (Table 1-1). Formation of calculi occurs when there is deposition of material in circumferential layers around a central nidus.(27) The nucleus of the stone may form from precipitation of supersaturated urine, precipitation of crystal on microscopic debris in the urine, or in the renal papilla which subsequently becomes exposed to urine through mucosal erosion and becomes a free calculus.(28) The central nucleus of the stone may differ in composition that the outer shell as factors that cause the formation of the nucleus of the stone may differ from the factors that cause stone growth.(28) The type of material deposited around the nidus varies with numerous factors, including urine pH and diet, which may change over time so the percentage of truly “pure” stones is reported to be 30-34%.(29, 30) Current methods typically classify a stone as a single substance if that substance comprises more than 60 - 75% of the total stone.(8, 14, 31) Therefore knowledge of the entire composition of the stone is essential to determine the etiological process and address preventing recurrence.(32)

Table 1-1 Chemical composition of common stones (28)

Full Name	Abbreviation	Chemical Composition
Calcium oxalate monohydrate (whewellite)	COM	$CaC_2O_4.H_2O$
Calcium oxalate dihydrate (weddellite)	COD	$CaC_2O_4.2H_2O$
Magnesium ammonium phosphate hexahydrate	MAP	$MgNH_4PO_4.6H_2O$
Carbonate – apatite	CAP	$Ca_{10}(PO_4,CO_3OH)_6(OH_2)$
Hydroxyl – apatite	HAP	$Ca_{10}(PO_4)_6(OH_2)$
Calcium hydrogen phosphate dihydrate (brushite)	BRU	$CaHPO_4.2H_2O$
Uric acid	UA	$C_5H_4N_4O_3$
Cystine	CYS	$[-SCH_2CH(NH_2)-COOH]_2$

The prevalence of the various stone types is somewhat region dependent but the following trends are noted. Calcium oxalate monohydrate and calcium oxalate dihydrate are two of the most common compounds found in human calculi representing more than 80% of all stones.(22, 28) Calcium hydrogen phosphate dihydrate (brushite) stones are uncommon occurring in less than 2% of stones.(28) Uric acid is found in 8-10% of stones. Cystine is uncommon occurring in 1-2% of stones.(28) Magnesium ammonium phosphate stones are typically associated with alkaline urine and urease splitting bacterial infections in people.(28) The imaging characteristics, fragility, and causative factors of common stones is given in Table 1-2.

Table 1-2 Characteristics of common calculi (1, 18, 33, 39)

Composition	**Radiographic Opacity**	**Attenuation (HU)**	**Fragility**	**Medically dissolvable**	**Etiological Factors**
Calcium monohydrate/ Calcium dehydrate	Moderate to markedly opaque	1700-2800	Moderate to very hard	No	Underlying metabolic disorder
Magnesium ammonium phosphate	Moderate to markedly opaque	1200-1600	Moderate	Yes	Renal infection
Urate	No to minimal radiopacity	200-450	Soft	Yes	Hyperuricemia
Cystine	Faint to moderate opacity	600-1100	Very hard	No	Renal tubular defect
Calcium Phosphate	Moderately to markedly opaque	Not reported	Moderate	No	None known
Silica	Moderate		unknown	No	
Brushite	Radiopaque	1700-2800	Very hard	No	Unknown

In dogs and cats magnesium ammonium phosphate and calcium oxalate stones are the most common stone type with an incidence of 39-53% and 35-45% respectively.(31, 33, 34) Urate stones are also common accounting for approximately 24% of stones submitted for analysis.(34) Although in veterinary medicine the overall incidence of urolithiasis has not changed over the past several decades there has been a dramatic shift in the type of stones identified with a decrease in magnesium ammonium phosphate stones and an increase in calcium oxalate stones. This is thought to be due to improvements in the dietary management of MAP stones. It is also theorized that diets that manage magnesium ammonium phosphate stones increase the risk of developing calcium oxalate stones.(31, 33, 34)

Because treatment of non obstructive stones varies with stone composition it is important to determine the composition in vivo.

1.2.3 Treatment options for urolithiasis

Treatment decisions for urinary calculi vary with the location, size, and composition of the stone (Figure 1-1). Stones located in the distal ureter and urinary bladder are most often removed via urethroscopy and cystoscopy. Large stones can be fragmented with concurrent use of laser lithotripsy to facilitate removal. Stones in the kidney and proximal ureter can be treated with ureteroscopy, surgery, percutaneous nephrolithotomy or extracorporeal shock wave lithotripsy. (18)

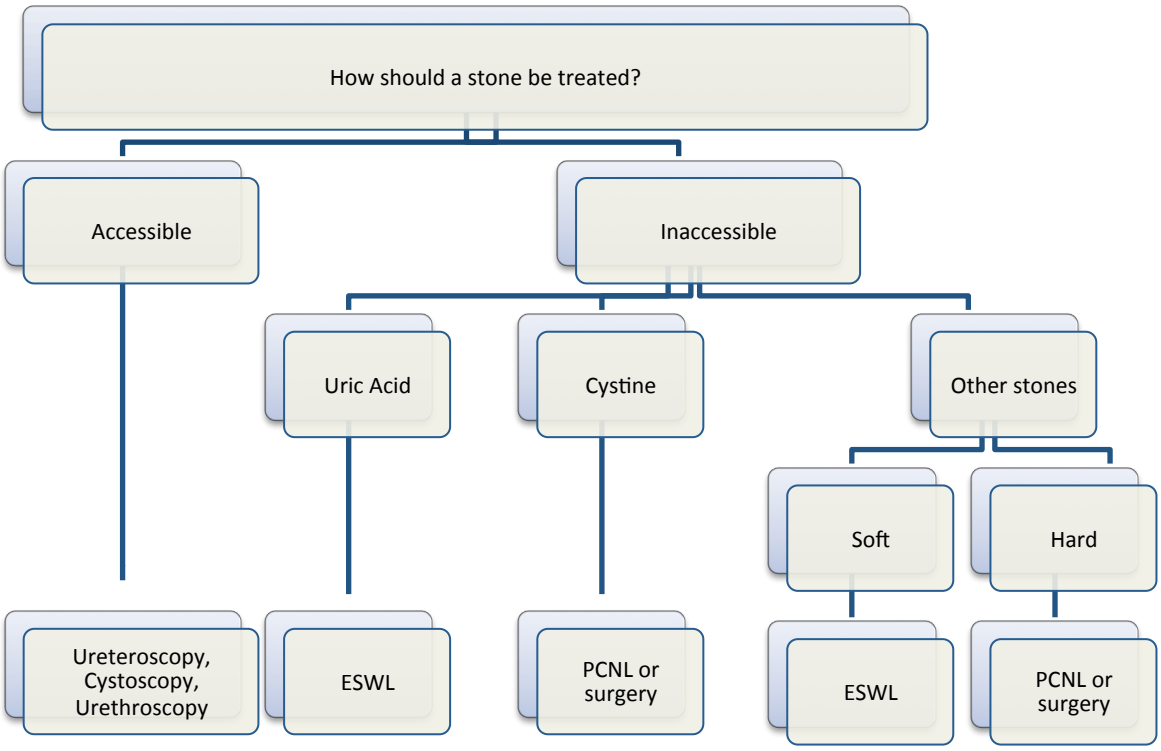

Figure 1-1: Overview of treatment options for urinary calculi based on location and stone composition (ESWL – extracorporeal shockwave lithotripsy, PCNL – percutaneous nephrolithotomy)

In recent years there have been considerable advances in the treatment of urolithiasis including intracorporal and extracorporeal shock wave lithotripsy. These techniques are advantageous in that they are minimally or non-invasive but not all stones are amenable to shock wave therapy. ESWL is unsuccessful in 9.4-26.3% of cases (35, 36) and is not without side effects including hypertension, renal function loss and an increase in stone recurrence rates, so it is important patients selected for this procedure have stones that are amenable to this treatment.(19) There can also be substantial cost associated with repeat treatment and alternative procedures when ESWL fails so it is important patients selected for this procedure have stones that are amenable to this treatment.(37, 38) As a result there has been considerable interest in developing in vivo assessments of stone composition and correlating stone composition with fragility and to allow for appropriate treatment decisions.

Uric acid stones are known for being soft and easily fragmented with shock wave therapy while brushite and cystine stones are harder and as a result are resistant to ESWL.(1, 39, 40) Struvite, uric acid and calcium oxalate dihydrate (COD) stones tend to fragment into small pieces while calcium oxalate monohydrate (COM) tends to fragment into larger pieces that are less likely to pass.(41) It has also been shown that within a specific chemical composition (particularly COM stones) there is great variability in stone fragility (co-efficient of variability 60%).(39) The reason for this variability is poorly understood but parameters that may influence stone fragility include composition, uniformity of composition, density, maximal diameter, total stone volume, and location in the urinary tract.(42-45) Within COM stones the concentration of magnesium, manganese and zinc were significantly lower in stones that were successfully fragmented with ESWL versus those that failed treatment.(41) Adams et.al. compared the fragility of calcium monohydrate stones from dogs and cats and found that feline stones were harder to break than canine stones in spite of the same chemical composition.(46) This may be due to varying amounts of organic material or a mix of minerals being present.(39) Mandhani et. al. used dual x-ray absorptiometry (DXA) to assess stone fragility and determined that fragility was correlated to stone mineral content and not mineral density. They hypothesized that a classification scheme that is independent of composition and based on stone mineral content would answer the clinically relevant question of whether

stones can be fragmented with ESWL or not.(38) In vivo work using single energy multidetector CT to evaluate the density of uroliths to classify according to this scheme was successful in classifying the stones in 66% of cases.(47, 48) Stones of greater than 1000 HU are significantly more likely to fail treatment by ESWL.(49) The majority of studies evaluate the stone on a single maximal diameter slice. Yoshida et. al. evaluated the entire stone volume and showed that although mean attenuation of the stone was significant in predicting successful ESWL the presence of a hump of high attenuation in the stone volume was the most accurate single predictive factor (positive predictive value 92.5%, negative predictive value 87.4%).(43) COM stones with a homogeneous internal architecture are significantly harder than those with a heterogeneous architecture requiring almost twice the number of shockwaves to fragment.(50)

Stone composition is important in treatment planning but stone site, stone size, stone number, history of urolithiasis, hydronephrosis, renal colic, and ureteral stents also affect the success rate of ESWL.(44, 45) If dual energy projection imaging can provide accurate information on the stone mineral content, regardless of the stone composition, then it may be a simple test to predict the effectiveness of ESWL.

1.2.4 Ex vivo methods of stone analysis

Ex vivo methods of stone analysis provide information that can be used for prevention of stone recurrence but not on treatment options and these tests are the standard to which all in vivo testing is compared.(51) However, currently there is no universally accepted standard for stone analysis.(51) Chemical analysis, polarized light microscopy, infrared spectroscopy and x-ray diffraction techniques are all used to analyze stones. These methods all require small powdered samples to analyze and that can limit the ability to differentiate the individual layers of the stone. Careful splitting the stone and analysis of samples from the different layers minimizes this limitation.(52) More recently coherent scatter CT and micro CT have been used to evaluate stones. These methods are non-destructive allowing for the identification of the layered composition in situ.

Chemical analysis can be performed to provide both a qualitative and quantitative assessment of stones.(53, 54) This provides a rough estimate of the constituents of a stone but there is some error as compounds may be present in several stone types (e.g. calcium and phosphate are present in brushite, whitelockite and octacalcium phosphate stones).(54)

All calculi are crystalline meaning there is an internal three-dimensional ordered structure of atoms. Polarized light microscopy can be used to identify the composition of stones because the transmission of light through a crystalline structure results in a unique pattern. The pattern from an unknown substance can be compared to patterns of known substances to determine its composition.(52) This method is cost effective, quick, and able to detect small components of mixed stones but is highly subjective and quantitative analysis is not possible.(29)

Infrared spectroscopy uses light to stimulate atomic vibration resulting in energy absorption. This is depicted as absorption bands in the infrared spectrum. The pattern of absorption bands can be compared to standards of pure samples to determine the composition. Mixed samples can also be evaluated, as the mixed spectrums are a simple overlay of the individual pure spectrums.(55, 56) This analysis can examine small samples, can detect the non crystalline components (fat or protein) and can be semi-automated.(29) Currently Fourier transform infrared spectroscopy (FTIR) and attenuated total internal reflection Fourier transform infrared spectroscopy (ATR-FTIR) are used for stone analysis. ATR-FTIR has the advantage of requiring less sample preparation. Measurements are independent of sample thickness so less grinding is required and ATR does not require mixing the sample with an infrared inactive material.(29, 57)

X-ray diffraction methods involve radiating a powdered sample with a monoenergetic beam. The x-rays are diffracted by the sample in a characteristic pattern. This provides a very robust method of accurately identifying the composition of stones and quantitate the components and is considered to be the gold standard in clinical stone analysis but is limited by the sample size.(58, 59) It was shown than in mixed stones if less than 5-15% of a compound was present it would not be detected with x-ray diffraction.(29, 52, 55)

An extension of the x-ray diffraction technique is coherent scatter computed tomography (CS-CT). Coherent scatter occurs when the x-ray photon interacts with the bound electrons causing them to vibrate resulting in the deflection the incident photon in a different direction. In the diagnostic energy range the photons scattered between 0-10° produce a material specific diffraction pattern.(60) X-ray diffraction cannot be used on thick samples because the randomly oriented crystallites result in complex scatter patterns. By using conventional filtered back projection techniques used in CT the average diffraction provides an average of diffraction spots over azimuthal angles that is equivalent to the analysis of powered samples.(58, 61, 62) Non destructive simultaneous evaluation of the stone composition and component distribution is the primary advantage of this method of analysis but it is currently only available at one institution.(63)

Micro CT provides excellent spatial resolution (to the micrometer) allowing for the determination of the internal architecture of stones including layers of components, irregularities in shape, and internal fissures. Because of its ability to differentiate the layers of the stone and rapidly scan numerous small fragments this method can be used to more accurately select samples for further analysis with FTIR or x-ray diffraction. Numerous small fragments can be assessed for their uniformity to determine how many and which fragments should undergo further analysis (64) Zarse et. al. showed that the components of common stones had differing attenuations that did not overlap.(65) This method is not being used commercially due to the high cost of the equipment but has numerous applications in the research of urolithiasis and the principles of micro-CT may eventually be able to be translated to clinical CT scanners for in vivo use.(64)

To aid in stone prevention accurate determination of all materials within a stone is important and although ex vivo methods of stone analysis will likely be more accurate than in vivo methods an in vivo test is still required to guide treatment decisions.

1.3 Dual energy imaging

To address the problem of in vivo determination of stone composition many have turned to dual energy CT. To date dual energy CT (DECT) has also shown inconsistent results.(Appendix A) Mostafavi et al. showed the dual energy ratio can be used to differentiate all stone types while several other authors could not reproduce these finding showing that calcium oxalate cannot be differentiated from brushite and MAP cannot be differentiated from silca.(4-8, 11-13, 15-17, 66) The trend in the literature is that dual energy CT can accurately differentiate between calcium containing, cystine, and urate stones but cannot differentiate MAP stones from other types and cannot differentiate between the types of calcium containing stones. To address these inconsistencies it is necessary to understand the principles of dual energy CT.

1.3.1 Principles of dual energy CT

Dual energy CT was first reported in the late 1970's but has not seen widespread use until recently due to limitations in CT technology.(67) This technique exploits the differences in the probability of the photoelectric and Compton interactions and the variability of K-edges between soft tissue, bone, and contrast medium when images are obtained at different energies.(21, 68-70) The CT number (H) [Hounsfield units] is a dimensionless quantity defined as

$$H \equiv 1000 \bullet \frac{\mu - \mu_w}{\mu_w} \tag{1.1}$$

where μ is the average linear attenuation coefficient [cm^{-1}] of the patient tissue and μ_w is the linear attenuation coefficient for water. The linear attenuation coefficient is the probability per cm of an x-ray photon interaction in a small thickness of tissue, which depends on the x-ray energy and average atomic number of patient tissue. A CT image therefore illustrates the relative difference of the linear attenuation coefficient of the patient tissue with respect to water. Imaging at different energies results in unique linear attenuation coefficients and therefore unique CT numbers.(67) The typical energy range

for diagnostic imaging is 60 to 140 kV. In this energy range there are two predominant interactions between the incident photon and the atom: the photoelectric effect and Compton scatter.

At the low energy range (<50 keV) the predominant interaction between the x-rays and the body is the photoelectric effect. The probability of the photoelectric effect occurring is proportional to Z^3/E^3 (Z = atomic number, E = energy of incident photon). The photoelectric effect predominates when low energy photons interact with high Z materials and, therefore, is a major contributor to the attenuation of high atomic number materials such as calcium, barium and iodine.(69, 71) A focal increase in attenuation due to photoelectric effect occurs just above the k-shell binding energy that is referred to as the k-edge. Above the k-edge energy the probability of the photoelectric effect is greater than just below the k-edge.(71) The k-edge energy is specific to each element and increases as the atomic number increases (Table 1-3). Because the k-edge is material specific, the photoelectric coefficient can provide information on the composition of the object.(70, 72)

Table 1-3 k-edge of common elements in the body and contrast agents (70)

Substance	Atomic Number (Z)	k-edge (keV)
Hydrogen	1	0.01
Carbon	6	0.28
Nitrogen	7	0.40
Oxygen	8	0.53
Calcium	20	4.00
Iodine	53	33.20
Barium	56	37.45
Gadolinium	64	50.20

Compton scatter predominates at energies >26 keV as the probability of a Compton interaction increases with the increasing energy of the incident photon. This interaction is also proportional to the electron density of the material and independent of Z making it the dominant interaction in soft tissue. In Compton scatter the incident photon interacts with and ejects an outer shell electron and the incident photon is scattered. The higher the energy of the incident photon the more likely the scattered photon will be in a forward direction and go on to interact with the detector. These scattered photons result in exposure of the image detector but do not reflect patient anatomy causing blurring in the image that decreases the contrast resolution.(71, 73)

Di Chiro et al. described the method for identifying tissue signatures with dual energy CT using the Compton and photoelectric components of the CT number as:

$$H = (H_C + \beta H_P)/(1+\beta) \qquad (1.2)$$

where H is the CT number, H_C the Compton number, H_P the photoelectric number, and β a quality or spectral factor obtained by calibration of the scanner.(74)

The composition of materials can be determined by dual energy imaging because there is a non linear relationship between effective linear attenuation coefficient for different materials at different energies. Figure 1-2 shows the linear attenuation curves of calcium and water. At energies used in diagnostic imaging (50 – 120 kV) these curves converge. The ratio of the attenuation coefficients obtained at two energies will be unique improving the delineation of materials with similar linear attenuation coefficients.

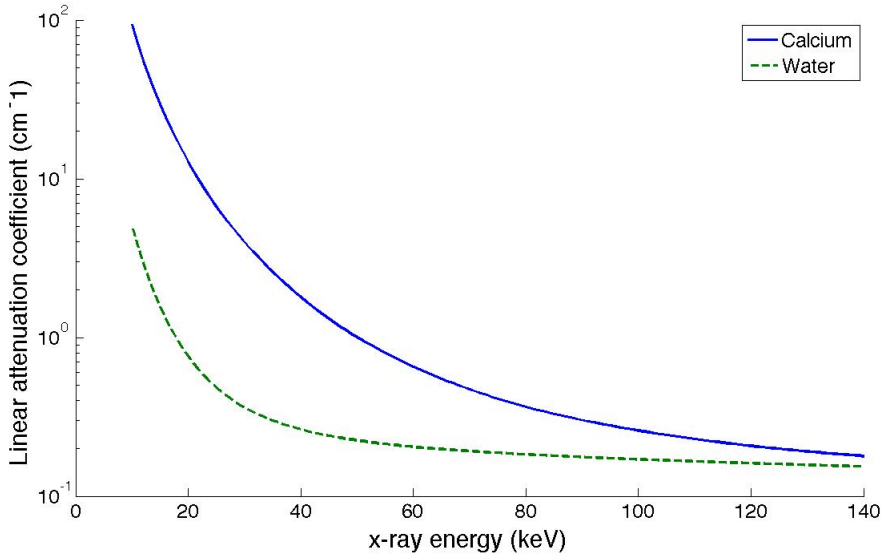

Figure 1-2: Linear attenuation coefficients of water and calcium from 10 to 120 kV

The most common dual energy measurements are the dual energy number (high energy CT number - the low energy CT number) or dual energy ratio (low energy CT number ÷ high energy CT number) with the latter being the most common method for classifying stone composition.(8, 49, 66) Figure 1-2 illustrates the effective linear attenuations coefficients of two materials at specific energies, but in conventional CT imaging, the beam is a spectrum and not monoenergetic so the degree of separation of these curves will be reduced which will have a negative impact on the ability to discriminate materials.

1.3.2 Methods used in dual energy imaging

Dual energy projection imaging can be performed by multiple methods: acquiring two consecutive scans with different energies, acquiring two images in rapid succession with differing kV, using a single shot technique with a dual peak x-ray spectrum, using a single shot technique using a dual energy detector that differentially absorbs the high and low energy spectrum, and simultaneous acquisition of dual energy scans with specialized CT scanners.(75-79)

The advantage of the dual exposure technique is the flexibility to optimize the energy separation between the images. Until recently the dual shot x-ray approach has only been used with a line scan technique with modified CT scanners or with consecutive acquisition of two series.(79-82) These techniques can result in inaccurate image registration and subsequent errors in the dual energy values. Recently the technology has developed that allows the acquisition of two images in rapid succession with an x-ray generator that can rapidly switch between two kV's. Regardless of acquisition method the potential downside to a dual exposure technique is an increase in patient dose. However, recent work has shown that high quality dual energy images can be produced using the same dose as a single DR image and the patient dose can still be less than or equivalent to conventional CT.(83, 84)

A method has been described to create a dual peak x-ray by using a 300 mg/cm^2 gadolinium filter at the tube output. Gadolinium has a favourable location of the K-edge making it an effective filter to create a dual peaked energy spectrum. However, in order to compensate for the beam filtration the current exposure product (mAs) needed to be increased ten-fold resulting in excessive patient dose.(75) An alternative method of obtaining a dual energy image is to use a single shot polyenergetic x-ray beam and two detectors that are separated by a filter. The first detector absorbs the low energy photons, the filter stops the remaining low energy photons, and the second detector absorbs the high energy photons.(75, 77) The advantage of these single shot techniques is that there is no possibility of patient movement between the two images, which had been the limiting

factor in dual shot techniques. Any patient movement will cause misregistration of the two images resulting in increased image error.(78) The disadvantage of these single shot techniques is in creating adequate energy separation between the two detectors to obtain high quality images. Greater energy separation between the images results in improved quality subtracted images. Initially images generated with this technique had poor quality but that was overcome by others that subsequently showed this technique can be used to generate images of sufficient diagnostic quality for clinical application. Even with the decreased signal to noise ratio (SNR), the subtracted images were superior to plain images in the detection of pulmonary nodules, pulmonary calcification, and rib lesions.(75, 77, 85)

One of the most important factors in determining image quality for dual energy subtracted images is the separation in the energy spectrum, particularly with K-edge techniques.(86) Having minimal energy overlap between the spectra is important to optimize bone or contrast cancellation.(84) Additionally, increasing the energy separation results in improved signal to noise ratio.(83) Obtaining adequate separation has been one of the challenges with a single shot technique. Using the gadolinium pre filter and sandwiched detectors the energy separation was approximately 23 keV while using the dual energy detectors it was 15 -23.6 keV.(75, 77, 78) Dual shot techniques allow for greater control over the separation in the energy spectrum and therefore improved decomposition analysis.

The cost of dual energy projection imaging is increased quantum noise.(76, 87, 88) In the diagnostic energy range only 1-10% of the total attenuation is due to the photoelectric effect.(89) In order to maximize the photoelectric effect lower energies are required and the lower energy photons cannot penetrate the tissues to expose the detector resulting in a decreased signal to noise ratio. At an equivalent x-ray dose the SNR is significantly lower.(87) Additionally the scatter patterns at high and low energies do not match. When creating a weighted subtracted image these mismatched scatter patterns will not cancel to zero resulting in increased error.(90) However it has been shown that in thoracic imaging anatomical noise, which is cancelled out in dual energy imaging, may be far greater than electronic noise and is a more important factor in limiting lesion detection.(91) The

reduction in anatomical noise likely more than compensates for the concurrent increase in quantum noise in dual energy images. However the question remains whether there is sufficient difference in the signal to noise ratio to accurately differentiate between different stone materials.

1.3.3 Controversy regarding ability of dual energy CT to determine stone composition

Numerous authors have evaluated the use of dual energy ratio and dual energy value as well as other CT parameters to determine stone composition with varied results. Mostafavi et al. and Saw et al. evaluated the density of stones with the high energy settings and showed that calcium containing stones could be differentiated from all other stones except brushite, and that magnesium ammonium phosphate stones could be differentiated from cystine stones.(5, 14) Other reports show dual energy ratio could differentiate all stones (12) or calcium containing stones from other stones (11, 66) while dual energy number could either differentiate all stones (5) or only uric acid from calcium oxalate and brushite (92). As discussed previously this may be due to a variety of factors including varied imaging parameters and criteria for a pure stone composition, differences in system calibration, scanner specific proprietary filters, beam hardening and partial volume averaging artifact. For example in a study by Graser et al. in 2008 an image of a stone composed of two materials is provided.(21) This image illustrates a linear band of material traversing the entire diameter of the stone. Formation of stones typically occurs by deposition of concentric rings around a central nidus. This linear deposition has never been reported and therefore this image may represent detection of an imaging artifact rather than a true difference in stone material. To address the differences noted in the literature it is necessary to determine the optimal imaging parameters for dual energy imaging and whether there is a fundamental difference in the signal to noise ratio between pure stone materials. If there is insufficient difference in the signal to noise ratio between pure stone materials in an ideal setting this technique will not be successful in a clinical setting.

1.3.4 Potential errors in dual energy CT

Potential reasons for the marked variability in the DECT results include errors in the CT measurements due to partial volume averaging, misregistration of the dual energy images (due to patient motion between images), CT scanner calibration errors, and beam hardening artifact.

Slice thickness and stone volume may be important factors in the ability of CT to accurately determine stone composition due to partial volume averaging.(49) Partial volume averaging occurs when materials of two or more different linear attenuation coefficients are included in the same voxel resulting in due to averaging. Partial volume averaging should not affect dual energy calculations as both the high and low energy measurements will be affected in a similar manner(13) with precise co-registration of the two x-ray beams. However, in small stones partial volume averaging may result in incorrect material characterization even with dual energy imaging because of inaccurate measurement of stone density.

Misregistration of the images was a potential source of error in the early work because the technology did not exist to acquire the images nearly simultaneously. Images were either acquired in two consecutive scans at different energies or alternating slices were acquired at different energies so the images were offset by the slice thickness. Dual energy CT scanners that can acquire images nearly simultaneously are now available so this is less likely to be a source of error in more recent studies.

CT scanners are calibrated to water and air and, therefore, should provide very consistent results for CT number determination. However, each scan protocol (i.e. each combination of mAs, kV, slice thickness, field of view, phantom diameter) is calibrated separately so if the calibration of the high and low energy scans is not consistent there may be variations in the CT number that artificially influence the dual energy values.

Beam hardening is an increase in the average energy of the incident beam due to the preferential attenuation of low energy photons. The degree of beam hardening will be

different for a high and low energy spectrum. Therefore, alternations in the linear attenuation coefficient between spectra of two energies may be due to artifact rather than differences in the material composition.

Monoenergetic beams do not suffer from beam hardening artifact and are better for performing material decomposition analysis. Monoenergetic beams are not possible in conventional CT scanners but beam filtration can be used to increase the spectral separation in dual energy scanning.(86) The only study of beam filtration for stone material discrimination is by Qu et al. where tin was used to filter the high energy beam and demonstrated improved discrimination of non-uric acid stones. (16) This work will determine the optimal task specific beam filtration for dual energy CT of urinary stones and determine whether there is a significant improvement in material discrimination with added filtration.

1.4 Research Goal

Our goal is to determine why there is a controversy in the previously reported dual energy result and to answer the question of whether there is sufficient difference in the signal to noise ratio of theoretical pure composition stone materials to discriminate between all stone materials that are amenable to ESWL and those that require surgical intervention in order to determine optimal treatment and reduce patient morbidity. Considerable effort has been spent on evaluating DECT for determining stone composition but published results show contradicting conclusions and a controversy remains as to whether this is even possible, and what stone materials can be identified. The goal of this research is to investigate the fundamental signals that DECT requires and make conclusions on how the DECT signal can be optimized. For example, the fundamental question of whether there is sufficient difference in the dual energy signal between stone materials has not been evaluated. If there is insufficient difference in the signal between pure stones then detecting differences in stones of mixed composition with systems that have inherent sources of error will never be effective. Task specific beam filtration to shape the spectra should also be evaluated to determine whether the use

of filtration can improve material discrimination. If there is sufficient difference in the dual energy signal to detect, this information can be used to optimize both DECT and determine the most effective method of using this information to determine stone composition.

1.5 Research Objectives

The hypothesis being tested is that there is adequate signal to noise difference in dual energy CT scans to distinguish between stone materials. The hypothesis will be tested with the following objectives:

1. Determine the fundamental dual energy signal to noise difference between different stone materials and determine whether there is sufficient difference between the signal to noise ratio to differentiate between the common stone materials.
2. Determine the optimal task specific beam filtration to increase the difference of the signal to noise ratio.
3. Perform a theoretical calculation of signal and noise for pure stone materials and make a conclusion about which materials can be separated with dual energy CT.
4. Determine the dual energy values for canine stones in a phantom and whether these values can be used to differentiate between various stone materials

1.6 Thesis outline

The goals of this thesis are addressed in two papers (chapters 2 and 3) that are in preparation for publication. The papers address the thesis objectives as described in the following section.

Chapter 2: Dual energy CT to predict urinary calculi composition: A theoretical model

To date there are variable and conflicting results with DECT for the prediction of urinary stone composition. To determine whether this is due to variations in study design a true in ability of DECT to answer the question of stone composition.

Chapter 2 describes a theoretical model to determine dual energy signal to noise ratio for pure stone materials using optimized spectra. Task specific beam filtration can be used to increase separation in beam spectra and therefore improve material discrimination. Using the theoretical model for dual energy SNR optimal beam filtration was determined and compared to unfiltered spectra for the discrimination of stone composition.

Chapter 3: Dual energy computed tomography of canine urinary calculi

Dual energy CT has not previously been used in veterinary medicine. Chapter 3 evaluated the use of dual energy CT in canine urinary calculi in a phantom. Dual energy values were compared to stone composition to determine whether dual energy values could be used to predict stone composition.

References:

1. Evan AP, Coe FL, Lingeman JE, Worcester E. Insights on the pathology of kidney stone formation. Urol Res. 2005;33(5):383-9.

2. Trinchieri A. Epidemiological trends in urolithiasis: impact on our health care systems. Urol Res. 2006;34(2):151-6.

3. Levine JA, Neitlich J, Verga M, Dalrymple N, Smith RC. Ureteral calculi in patients with flank pain: correlation of plain radiography with unenhanced helical CT. Radiology. 1997;204(1):27-31.

4. Demirel A, Suma S. The efficacy of non-contrast helical computed tomography in the prediction of urinary stone composition in vivo. J Int Med Res. 2003;31(1):1-5.

5. Mostafavi MR, Ernst RD, Saltzman B. Accurate determination of chemical composition of urinary calculi by spiral computerized tomography. J Urol. 1998;159(3):673-5.

6. Mitcheson HD, Zamenhof RG, Bankoff MS, Prien EL. Determination of the chemical composition of urinary calculi by computerized tomography. J Urol. 1983;130(4):814-9.

7. Hillman BJ, Drach GW, Tracey P, Gaines JA. Computed tomographic analysis of renal calculi. AJR Am J Roentgenol. 1984;142(3):549-52.

8. Hidas G, Eliahou R, Duvdevani M, et al. Determination of renal stone composition with dual-energy CT: in vivo analysis and comparison with x-ray diffraction. Radiology. 2010;257(2):394-401.

9. Thomas C, Patschan O, Ketelsen D, et al. Dual-energy CT for the characterization of urinary calculi: In vitro and in vivo evaluation of a low-dose scanning protocol. Eur Radiol. 2009;19(6):1553-9.

10. Thomas C, Heuschmid M, Schilling D, et al. Urinary calculi composed of uric acid, cystine, and mineral salts: differentiation with dual-energy CT at a radiation dose comparable to that of intravenous pyelography. Radiology. United States: Rsna, 2010., 2010; p. 402-9.

11. Graser A, Johnson TR, Bader M, et al. Dual energy CT characterization of urinary calculi: initial in vitro and clinical experience. Invest Radiol. 2008;43(2):112-9.

12. Boll DT, Patil NA, Paulson EK, et al. Renal stone assessment with dual-energy multidetector CT and advanced postprocessing techniques: improved characterization of renal stone composition--pilot study. Radiology. 2009;250(3):813-20.

13. Primak AN, Fletcher JG, Vrtiska TJ, et al. Noninvasive differentiation of uric acid versus non-uric acid kidney stones using dual-energy CT. Acad Radiol. 2007;14(12):1441-7.

14. Saw KC, McAteer JA, Monga AG, Chua GT, Lingeman JE, Williams JC, Jr. Helical CT of urinary calculi: effect of stone composition, stone size, and scan collimation. AJR Am J Roentgenol. 2000;175(2):329-32.

15. Qu M, Jaramillo-Alvarez G, Ramirez-Giraldo JC, et al. Urinary stone differentiation in patients with large body size using dual-energy dual-source computed tomography. Eur Radiol. 2013;23(5):1408-14.

16. Qu M, Ramirez-Giraldo JC, Leng S, et al. Dual-energy dual-source CT with additional spectral filtration can improve the differentiation of non-uric acid renal stones: an ex vivo phantom study. AJR Am J Roentgenol. 2011;196(6):1279-87.

17. Wang J, Qu M, Duan X, et al. Characterisation of urinary stones in the presence of iodinated contrast medium using dual-energy CT: a phantom study. Eur Radiol. 2012;22(12):2589-96.

18. Kambadakone AR, Eisner BH, Catalano OA, Sahani DV. New and evolving concepts in the imaging and management of urolithiasis: urologists' perspective. Radiographics. 2010;30(3):603-23.

19. Stoller M, Meng M. Urinary stone disease: the practical guide to medical and surgical management. Towata, New Jersey: Humana Press, 2007.

20. Turgut M, Unal I, Berber A, Demir TA, Mutlu F, Aydar Y. The concentration of Zn, Mg and Mn in calcium oxalate monohydrate stones appears to interfere with their fragility in ESWL therapy. Urological Research. 2008;36(1):31-8.

21. Graser A, Johnson TRC, Bader M, et al. Dual energy CT characterization of urinary calculi: initial in vitro and clinical experience. Invest Radiol. 2008;43(2):112-9.

22. Knoll T. Epidemiology, pathogenesis, and pathophysiology of urolithiasis. European urology supplements. 2010;9(12):802.

23. Merck, Co. The Merck veterinary manual: a handbook of diagnosis, therapy and disease prevention and control for the veterinarian. 7th ed. Ragway: Merck & Co., 1991.

24. Ramakumar S, Patterson DE, LeRoy AJ, et al. Prediction of stone composition from plain radiographs: a prospective study. J Endourol. 1999;13(6):397-401.

25. Oehlschläger S, Hakenberg OW, Froehner M, Manseck A, Wirth MP. Evaluation of chemical composition of urinary calculi by conventional radiography. J Endourol. 2003;17(10):841-5.

26. Krishnamurthy MS, Ferucci PG, Sankey N, Chandhoke PS. Is stone radiodensity a useful parameter for predicting outcome of extracorporeal shockwave lithotripsy for stones < or = 2 cm? Int Braz J Urol. 2005;31(1):3-8.

27. Rodgers AL, Nassimbeni LR, Mulder KJ. A multiple technique approach to the analysis of urinary calculi. Urol Res. 1982;10(4):177-84.

28. Prien EL, Prien EL. Composition and structure of urinary stone. The American journal of medicine. 1968;45(5):654-72.

29. Schubert G. Stone analysis. Urol Res. 2006;34(2):146-50.

30. Daudon M, Donsimoni R, Hennequin C, et al. Sex- and age-related composition of 10 617 calculi analyzed by infrared spectroscopy. Urol Res. 1995;23(5):319-26.

31. Houston DM, Moore AE. Canine and feline urolithiasis: examination of over 50 000 urolith submissions to the Canadian veterinary urolith centre from 1998 to 2008. Can Vet J. 2009;50(12):1263-8.

32. Daudon M, Bader CA, Jungers P. Urinary calculi: review of classification methods and correlations with etiology. Scanning Microsc. 1993;7(3):1081-104; discussion 104-6.

33. Ettinger S, Feldman E. Textbook of Veterinary Internal Medicine: Elsevier - Health Sciences Division, 2004.

34. Low WW, Uhl JM, Kass PH, Ruby AL, Westropp JL. Evaluation of trends in urolith composition and characteristics of dogs with urolithiasis: 25,499 cases (1985-2006). J Am Vet Med Assoc. 2010;236(2):193-200.

35. Logarakis NF, Jewett MA, Luymes J, Honey RJ. Variation in clinical outcome following shock wave lithotripsy. J Urol. 2000;163(3):721-5.

36. Ehreth JT, Drach GW, Arnett ML, et al. Extracorporeal shock wave lithotripsy: multicenter study of kidney and upper ureter versus middle and lower ureter treatments. J Urol. 1994;152(5 Pt 1):1379-85.

37. Joseph P, Mandal AK, Singh SK, Mandal P, Sankhwar SN, Sharma SK. Computerized tomography attenuation value of renal calculus: can it predict successful fragmentation of the calculus by extracorporeal shock wave lithotripsy? A preliminary study. J Urol. 2002;167(5):1968-71.

38. Mandhani A, Raghavendran M, Srivastava A, et al. Prediction of fragility of urinary calculi by dual X-ray absorptiometry. J Urol. 2003;170(4 Pt 1):1097-100.

39. Williams JC, Jr., Saw KC, Paterson RF, Hatt EK, McAteer JA, Lingeman JE. Variability of renal stone fragility in shock wave lithotripsy. Urology. United States2003; p. 1092-6; discussion 7.

40. Ansari MS, Gupta NP, Seth A, Hemal AK, Dogra PN, Singh TP. Stone fragility: its therapeutic implications in shock wave lithotripsy of upper urinary tract stones. Int Urol Nephrol. 2003;35(3):387-92.

41. Turgut M, Unal I, Berber A, Demir TA, Mutlu F, Aydar Y. The concentration of Zn, Mg and Mn in calcium oxalate monohydrate stones appears to interfere with their fragility in ESWL therapy. Urol Res. 2008;36(1):31-8.

42. Kijvikai K, de la Rosette JJ. Assessment of stone composition in the management of urinary stones. Nat Rev Urol. 2011;8(2):81-5.

43. Yoshida S, Hayashi T, Ikeda J, et al. Role of volume and attenuation value histogram of urinary stone on noncontrast helical computed tomography as predictor of fragility by extracorporeal shock wave lithotripsy. Urology. 2006;68(1):33-7.

44. Gupta NP, Ansari MS, Kesarvani P, Kapoor A, Mukhopadhyay S. Role of computed tomography with no contrast medium enhancement in predicting the outcome of extracorporeal shock wave lithotripsy for urinary calculi. BJU Int. 2005;95(9):1285-8.

45. Wang M, Shi Q, Wang X, Yang K, Yang R. Prediction of outcome of extracorporeal shock wave lithotripsy in the management of ureteric calculi. Urol Res. 2011;39(1):51-7.

46. Adams LG, Williams JC, McAteer JA, Hatt EK, Lingeman JE, Osborne CA. In vitro evaluation of canine and feline calcium oxalate urolith fragility via shock wave lithotripsy. Am J Vet Res. 2005;66(9):1651-4.

47. Chevreau G, Troccaz J, Conort P, et al. Estimation of urinary stone composition by automated processing of CT images. Urol Res. 2009;37(5):241-5.

48. Zarse CA, McAteer JA, Tann M, et al. Helical computed tomography accurately reports urinary stone composition using attenuation values: in vitro verification using high-resolution micro-computed tomography calibrated to fourier transform infrared microspectroscopy. Urology. 2004;63(5):828-33.

49. El-Assmy A, Abou-El-Ghar ME, El-Nahas AR, Refaie HF, Sheir KZ. Multidetector Computed Tomography: Role in Determination of Urinary Stones Composition and Disintegration With Extracorporeal Shock Wave Lithotripsy-an in Vitro Study. Urology. 2011;77(2):286-90.

50. Zarse CA, Hameed TA, Jackson ME, et al. CT visible internal stone structure, but not Hounsfield unit value, of calcium oxalate monohydrate (COM) calculi predicts lithotripsy fragility in vitro. Urol Res. 2007;35(4):201-6.

51. Krambeck AE, Khan NF, Jackson ME, Lingeman JE, McAteer JA, Williams JC, Jr. Inaccurate reporting of mineral composition by commercial stone analysis laboratories: implications for infection and metabolic stones. J Urol. United States: Inc. Published by Elsevier Inc, 2010; p. 1543-9.

52. Prien EL, Prien EL, Jr. Composition and structure of urinary stone. Am J Med. United States1968; p. 654-72.

53. Asper R. Stone analysis. Urol Res. 1990;18 Suppl 1:S9-12.

54. Hodgkinson A. A combined qualitative and quantitative procedure for the chemical analysis of urinary calculi. J Clin Pathol. 1971;24(2):147-51.

55. Weissman M, Klein B, Berkowitz J. Clinical applications of infrared spectroscopy: Analysis of renal tract calculi. Analytical Chemistry. 1959;31(8):1334-8.

56. Chen WC, Wu SY, Liu HP, et al. Identification of melamine/cyanuric acid-containing nephrolithiasis by infrared spectroscopy. J Clin Lab Anal. 2010;24(2):92-9.

57. Gulley-Stahl HJ, Haas JA, Schmidt KA, Evan AP, Sommer AJ. Attenuated total internal reflection Fourier transform infrared spectroscopy: a quantitative approach for kidney stone analysis. Appl Spectrosc. 2009;63(7):759-66.

58. Davidson MT, Batchelar DL, Velupillai S, Denstedt JD, Cunningham IA. Analysis of urinary stone components by x-ray coherent scatter: characterizing composition beyond laboratory x-ray diffractometry. Phys Med Biol. 2005;50(16):3773-86.

59. Prien EL, Frondel C. Studies in urolithiasis; the composition of urinary calculi. J Urol. 1947;57(6):949-94.

60. Johns PC, Yaffe MJ. Coherent scatter in diagnostic radiology. Med Phys. 1983;10(1):40-50.

61. Westmore MS, Fenster A, Cunningham IA. Tomographic imaging of the angular-dependent coherent-scatter cross section. Med Phys. 1997;24(1):3-10.

62. Batchelar DL, Cunningham IA. Material-specific analysis using coherent-scatter imaging. Med Phys. 2002;29(8):1651-60.

63. Davidson MT, Batchelar DL, Chew BH, Denstedt JD, Cunningham IA. Establishing composition and structure of intact urinary calculi by x-ray coherent scatter for clinical laboratory investigations. J Urol. 2006;175(6):2336-40.

64. Williams JC, McAteer JA, Evan AP, Lingeman JE. Micro-computed tomography for analysis of urinary calculi. Urol Res. 2010;38(6):477-84.

65. Zarse CA, McAteer JA, Sommer AJ, et al. Nondestructive analysis of urinary calculi using micro computed tomography. BMC Urol. 2004;4(1):15.

66. Thomas C, Heuschmid M, Schilling D, et al. Urinary calculi composed of uric acid, cystine, and mineral salts: differentiation with dual-energy CT at a radiation dose comparable to that of intravenous pyelography. Radiology. 2010;257(2):402-9.

67. Silva AC, Morse BG, Hara AK, Paden RG, Hongo N, Pavlicek W. Dual-energy (spectral) CT: applications in abdominal imaging. Radiographics. 2011;31(4):1031-46.

68. Richard S, Siewerdsen JH, Jaffray DA, Moseley DJ, Bakhtiar B. Generalized DQE analysis of radiographic and dual-energy imaging using flat-panel detectors. Med Phys. 2005;32(5):1397-413.

69. Brody WR, Butt G, Hall A, Macovski A. A method for selective tissue and bone visualization using dual energy scanned projection radiography. Med Phys. 1981;8(3):353-7.

70. Coursey CA, Nelson RC, Boll DT, et al. Dual-energy multidetector CT: how does it work, what can it tell us, and when can we use it in abdominopelvic imaging? Radiographics. United States2010; p. 1037-55.

71. Bushberg J. The essential physics of medical imaging: Lippincott Williams & Wilkins, 2012.

72. Alvarez RE, Macovski A. Energy-selective reconstructions in X-ray computerized tomography. Phys Med Biol. 1976;21(5):733-44.

73. Bushberg JT. The AAPM/RSNA physics tutorial for residents. X-ray interactions. Radiographics. 1998;18(2):457-68.

74. Di Chiro G, Brooks R, Kessler R. Tissue signatures with dual-energy computed tomography. Radiology. 1979;131:521-3.

75. Ergun DL, Mistretta CA, Brown DE, et al. Single-exposure dual-energy computed radiography: improved detection and processing. Radiology. 1990;174(1):243-9.

76. Lehmann LA, Alvarez RE, Macovski A, et al. Generalized image combinations in dual KVP digital radiography. Med Phys. 1981;8(5):659-67.

77. Ishigaki T, Sakuma S, Horikawa Y, Ikeda M, Yamaguchi H. One-shot dual-energy subtraction imaging. Radiology. 1986;161(1):271-3.

78. Barnes GT, Sones RA, Tesic MM, Morgan DR, Sanders JN. Detector for dual-energy digital radiography. Radiology. 1985;156(2):537-40.

79. Marin D, Boll DT, Mileto A, Nelson RC. State of the art: dual-energy CT of the abdomen. Radiology. 2014;271(2):327-42.

80. Brody WR, Cassel DM, Sommer FG, et al. Dual-energy projection radiography: initial clinical experience. AJR Am J Roentgenol. 1981;137(2):201-5.

81. Sommer FG, Brody WR, Gross D, Macovski A, Hall A, Pelc N. Excretory urography using dual-energy scanned projection radiography. Radiology. 1981;141(2):529-32.

82. Sommer FG, Brody WR, Gross D, Macovski A. Renal imaging with dual energy projection radiography. AJR Am J Roentgenol. 1982;138(2):317-22.

83. Shkumat NA, Siewerdsen JH, Dhanantwari AC, et al. Optimization of image acquisition techniques for dual-energy imaging of the chest. Med Phys. 2007;34(10):3904-15.

84. Richard S, Siewerdsen JH. Optimization of dual-energy imaging systems using generalized NEQ and imaging task. Med Phys. 2007;34(1):127-39.

85. Ishigaki T, Sakuma S, Ikeda M. One-shot dual-energy subtraction chest imaging with computed radiography: clinical evaluation of film images. Radiology. 1988;168(1):67-72.

86. Primak AN, Ramirez Giraldo JC, Liu X, Yu L, McCollough CH. Improved dual-energy material discrimination for dual-source CT by means of additional spectral filtration. Med Phys. 2009;36(4):1359-69.

87. Warp RJ, Dobbins JT. Quantitative evaluation of noise reduction strategies in dual-energy imaging. Med Phys. 2003;30(2):190-8.

88. Kelcz F, Zink FE, Peppler WW, Kruger DG, Ergun DL, Mistretta CA. Conventional chest radiography vs dual-energy computed radiography in the detection and characterization of pulmonary nodules. AJR Am J Roentgenol. 1994;162(2):271-8.

89. Avrin DE, Macovski A, Zatz LE. Clinical application of Compton and photo-electric reconstruction in computed tomography: preliminary results. Invest Radiol. 1978;13(3):217-22.

90. Riederer SJ. Performance of x-ray imaging systems applied to intravenous angiography. IEEE Trans Med Imaging. 1982;1(1):48-62.

91. Samei E, Flynn MJ, Eyler WR. Detection of subtle lung nodules: relative influence of quantum and anatomic noise on chest radiographs. Radiology. 1999;213(3):727-34.

92. Matlaga BR, Kawamoto S, Fishman E. Dual source computed tomography: a novel technique to determine stone composition. Urology. 2008;72(5):1164-8.

Chapter 2 – Dual energy CT to predict urinary calculi composition: A theoretical model

This chapter is will be submitted to Radiology.

2.1 Introduction

Urolithiasis is a common problem in people with a prevalence of 3-20% worldwide.(1) Selection of the ideal treatment is dependent on the composition of the stone; therefore, it would be extremely helpful to have an in vivo method of determining stone composition. Considerable effort has been spent on evaluating dual energy CT for determining stone composition with inconsistent results.(2-15) These studies evaluated one or more of the following measures: the CT number of the stone with the high energy beam, the dual energy number (low energy CT number – high energy CT number, or the dual energy ratio (low energy CT number ÷ high energy CT number. The results of these studies are varied with the only consistent finding from these studies is that uric acid stones can be differentiated from other stones. Mostafavi et al. and Saw et al. evaluated the density of stones with the high energy settings and showed that calcium containing stones could be differentiated from all other stones except brushite, and that magnesium ammonium phosphate stones could be differentiated from cystine stones.(3, 12) Dual energy ratio could differentiate all stones (10) and calcium containing stones from other stones (9, 16), while dual energy number could either differentiate all stones (3) or only uric acid from calcium oxalate and brushite (17). Inconsistency in these results may be due to variability in study design. Energy settings ranged from 77 to 140 kV and mAs settings ranged from 23 to 747 with ratios of the high and low mAs from 1:1 to 1:4.6. Stone analysis methodology and purity of the stone varied among the studies ranging from 60% to 90% pure and stones were of various sizes. System calibration, scanner specific

proprietary filters, beam hardening and partial volume averaging artifact may also influence reported measurements. Therefore, the question remains whether it is fundamentally possible to determine stone composition with dual energy CT.

Task specific optimization of the beam filtration for dual energy imaging has been done for chest radiographs and mammography and general CT.(18-20) The only study of beam filtration for stone material discrimination is by Qu et al. where tin was used to filter the high energy beam. This study demonstrated improved discrimination of non-uric acid stones but did not facilitate discrimination of calcium oxalate monohydrate, calcium oxalate dihydrate and brushite stones.(14) To our knowledge task specific optimization of CT for determining stone composition has not been done previously. Added filtration changes the shape of the spectrum and increases the spectral separation between the low and high energy beams which should increase the accuracy of the dual energy values and improve the ability to differentiate between stones of differing compositions. (20, 21)

The hypothesis is that there is adequate signal to noise difference in a 3x3x1 mm voxel to distinguish between pure stone materials of a 1 cm volume and that the addition of task specific beam filtration will improve the ability to distinguish between different stone materials. This hypothesis was tested by: determining the optimal energy settings and beam filtration to maximize the difference in the dual energy measurement of urinary calculi for computed tomography, and determining whether there is adequate difference between the dual energy measurements to differentiate between pure composition stones in a pure stone theoretical model. Specifically it will be determined whether there is adequate difference in the dual energy number and dual energy ratio between stones that are amenable by shock wave lithotripsy and those that typically require nephrolithotomy.

2.2 Theory

Differentiating between stones of different composition requires maximizing the signal to noise ratio in the difference of the dual energy measurement between stones. The best results may require optimizing the user-controlled variables including energy of the spectra, mAs ratio, and beam filtration (material and thickness) for an acceptable patient

dose. For comparison the difference in the dual energy signal to noise ratio was standardized to the square root of the mean total entrance exposure providing a measure that was independent of patient dose. This calculation was developed for single slice axial scanners with filtered back projection but it is reasonable to assume that conditions that optimize this signal to noise ratio will also apply to a helical multi slice scanner and iterative reconstruction technologies.(22) Also, axial scans generally have superior slice separation to helical scans improving detection of subtle lesions.(22)

For a monoenergetic x-ray beam the CT number (H) [Hounsfield units] is a dimensionless quantity defined as

$$H \equiv 1000 \bullet \frac{\mu - \mu_w}{\mu_w} \tag{2.1}$$

where μ is the average linear attenuation coefficient [cm^{-1}] of the patient tissue and μ_w is the linear attenuation coefficient for water. The linear attenuation coefficient is the probability per cm of an x-ray photon interaction in a small thickness of tissue, which depends on the x-ray energy and average atomic number of patient tissue. A CT image therefore illustrates the relative difference of the linear attenuation coefficient of the patient tissue with respect to water.

The statistical variance in H, σ_H^2, is obtained by differentiating equation (2.1):

$$\begin{aligned} \sigma_H^2 &= \left|\frac{d}{d\mu}H\right|^2 \sigma_\mu^2 + \left|\frac{d}{d\mu_w}H\right|\sigma_{\mu_w}^2 \\ &= \left|\frac{10^3}{\mu_w}\right|^2 \sigma_\mu^2 \end{aligned} \tag{2.2}$$

where $\sigma_{\mu_w}^2$ is assumed negligible since CT scanners use multiple scans to perform an accurate determinant of μ_w during regular system calibrations. Figure 2-1 illustrates the geometry of a fan beam third generation CT scanner.

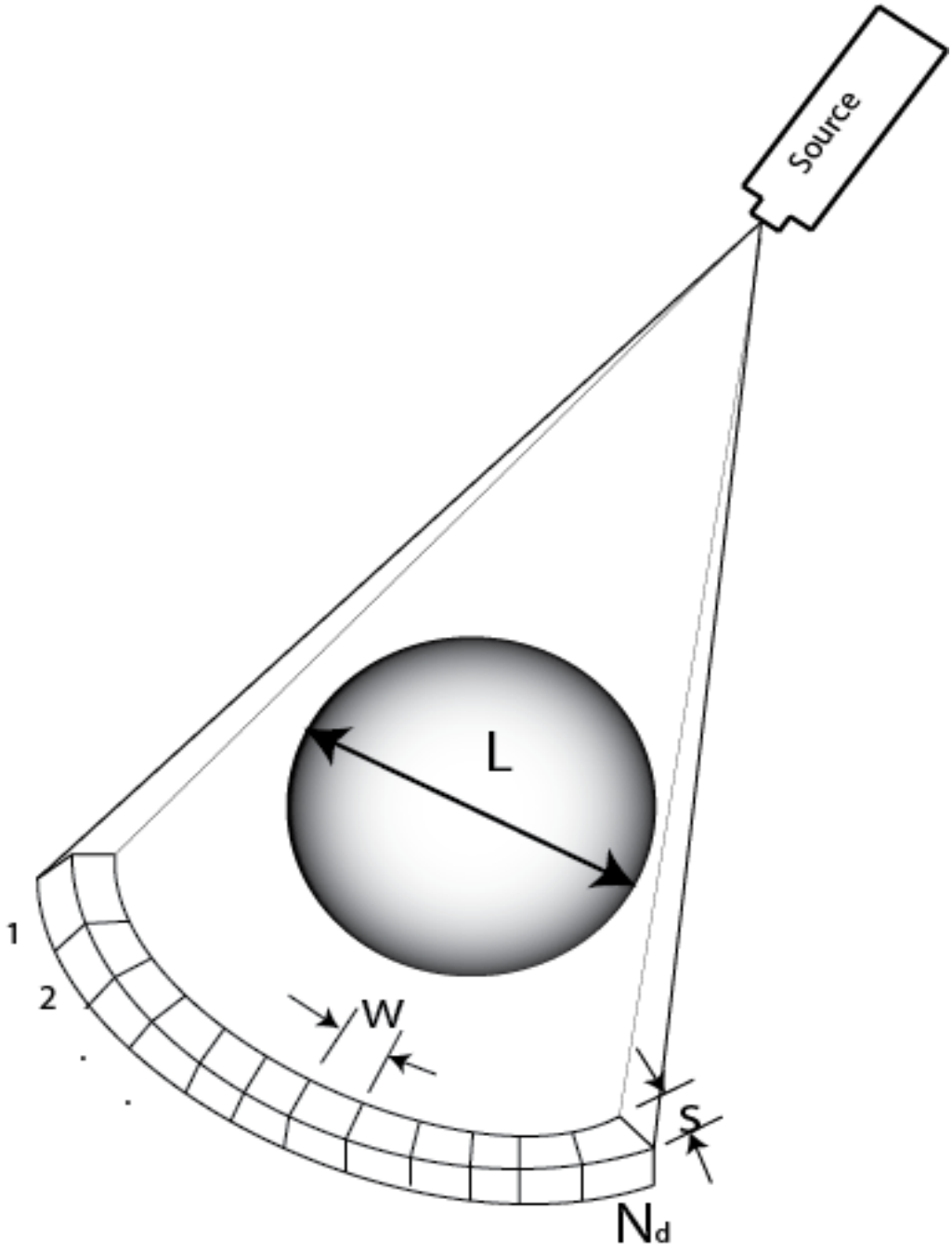

Figure 2-1 Schematic of a fan beam geometry CT scanner where L = phantom diameter, w = the detector width [cm], s = slice thickness [cm], and N_d = number of detectors.

Faulkner and Moores described the noise in the CT number for this geometry as calculated in Appendix F giving [cm^{-2}] (23, 24):

$$\sigma_{\mu}^{2} = \frac{\pi}{12w^{2}e^{-\mu L}[Q_{0}Iws]\varepsilon} \tag{2.3}$$

where Q_0 [cm^{-2} mAs^{-1}] is the normalized density of photons incident on the detector along the central ray of each projection measurement when no phantom is present, I [mAs] is the product of tube current and exposure time for one 360° rotation of the x-ray tube, w [cm] the width of the detector, s [cm] is the slice thickness, and ε is the detector quantum efficiency. The statistical variance in the CT number is therefore given by (23, 25) [unitless]:

$$\sigma_{H}^{2} = \frac{10^{6}\pi}{12w^{3}s}\frac{1}{Q_{0}I\mu_{w}^{2}e^{-\mu L}\varepsilon}. \tag{2.4}$$

This calculation considers only x-ray quantum noise as it is propagated to the CT images for a circular phantom of uniform material and density, which is a good approximation for normally exposed soft tissue images with a monoenergetic x-ray source, but does not include noise from scatter radiation.

This simple model has been effective is developing an understanding of noise in CT images for filtered back projection reconstruction using a ramp filter (Shepp-Logan) for ideal detector elements.(23) However, it is not sufficient to assume a monoenergetic spectrum for dual-energy imaging, particularly when considering special filtration to increase the energy separation of high and low energy spectra to maximize dual energy values for particular applications. Following the approach of Faulkner and Kelcz, we developed an expression for the CT variance in equation (2.4) generalized for an arbitrary x-ray spectrum Q_0(E), and detector quantum efficiency ε(E) giving

$$\sigma_{H}^{2} = \frac{10^{6}\pi^{2}}{12w^{2}ws\mu_{w}^{2}}\frac{\int_{0}^{kV} Q_{0}(E)IE^{2}\varepsilon(E)dE}{\left[\int_{0}^{kV} Q(E)IE\ \varepsilon(E)dE\right]^{2}}. \tag{2.5}$$

Dual energy signals can be calculated multiple ways but dual energy number (S_N) and dual energy ratio (S_R) are the most common and they are easy to calculate: (10, 17, 26-28)

$$S_N = H_L - H_H \tag{2.6}$$

$$S_R = \frac{H_L}{H_H} \tag{2.7}$$

To compare optimal energy and filter settings, we use a figure of merit that expresses the signal to noise ratio (SNR) for dual energy number and ratio for two selected stone materials assuming the same dose (D) at the isocentre of a circular phantom. Measurements of the CT number for the high and low energy spectra are obtained from different scans and hence are statistically uncorrelated, giving the figure of merit for the dual energy number (F_N^2) and dual energy ratio (F_R^2) as [mGy]:

$$F_N^2 = \frac{\left|S_{Na} - S_{Nb}\right|^2 \Big/ \left(\sigma_{S_{Na}}^2 + \sigma_{S_{Nb}}^2\right)}{D} \tag{2.8}$$

and

$$F_R^2 = \frac{\left|S_{Ra} - S_{Rb}\right|^2 \Big/ \left(\sigma_{S_{Ra}}^2 + \sigma_{S_{Rb}}^2\right)}{D} \tag{2.9}$$

where the subscripts a and b represent different materials. Propagation of error through Eq. (2.6) and (2.7) gives the uncertainties in S_N and S_R as [unitless]:

$$\sigma_{S_N}^2 = \sigma_{H_H}^2 + \sigma_{H_L}^2 \tag{2.10}$$

and

$$\sigma_{S_R}^2 = \frac{1}{H_H^2}\left(\sigma_{H_L}^2 + S_R^2\sigma_{H_H}^2\right). \quad (2.11)$$

The isocentre dose D in the phantom is estimated for each spectrum using a CT KERMA-ratio method described by Huda.(29) Using air KERMA values measured at selected locations in a Rando phantom (K) and at isocentre with the phantom removed (K_{CT}), he determined the ratio $R_K \equiv K/K_{CT}$ for selected techniques on a GE Lightspeed Ultra. (30, 31) The abdominal dose is therefore given by D [mGy]:

$$D = K \bullet \frac{\left(\frac{\mu_{ab}}{\rho}\right)_{med}}{\left(\frac{\mu_{ab}}{\rho}\right)_{air}} = K_{CT} \bullet R_K \bullet \frac{\left(\frac{\mu_{ab}}{\rho}\right)_{med}}{\left(\frac{\mu_{ab}}{\rho}\right)_{air}} \quad . \quad (2.12)$$

where μ_{ab}/ρ is the mass energy absorption in the patient and air. Using R_K values determined by Huda et al. at 80, 120, and 140 kV, and the half value layer of these spectra measured by Mathieu et al., (32) a least squares linear regression was generated to calculate R_K as a function of half value layer showing a linear relationship between R_K and HVL. The HVL of spectra used in this study are determined from this relationship as illustrated in (Figure 2-2).

.

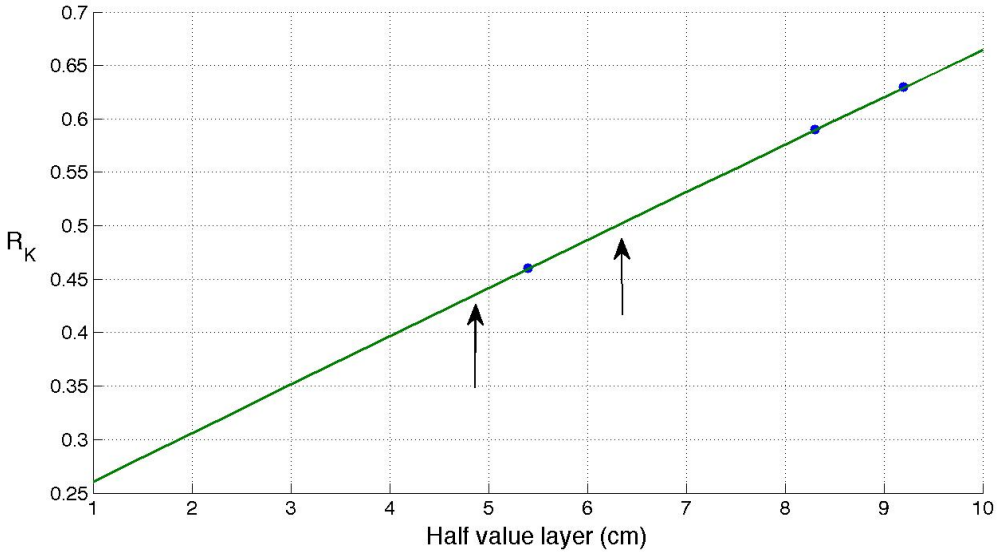

Figure 2-2 Plot of best fit linear model of R_K to half value layer (line) based on measured values from Huda et al. and Matheiu et al. (dots). The arrows indicate the half value layer of the low and high energy beams used in this study.

The chemical composition of the stone materials used in the analysis are provided in Table 2-1.

Table 2-1 Stone material specifications (33)

Full Name	Abbreviation	Chemical Composition
Calcium oxalate monohydrate (whewellite)	COM	$CaC_2O_4.H_2O$
Calcium oxalate dihydrate (weddellite)	COD	$CaC_2O_4.2H_2O$
Magnesium ammonium phosphate hexahydrate	MAP	$MgNH_4PO_4.6H_2O$
Hydroxyapatite	HAP	$Ca_{10}(PO_4)_6(OH_2)$
Calcium hydrogen phosphate dihydrate (brushite)	BRU	$CaHPO_4.2H_2O$
Uric acid	US	$C_5H_4N_4O_3$
Cystine	CYS	$[-SCH_2CH(NH_2)-COOH]_2$

2.3 Materials and Methods

Determination of optimal energy settings and whether added filtration can improve discrimination of stone composition with dual energy CT requires determination of the optimal filter material, based on theoretical modeling with the figure of merit. The ability to separate two materials based on dual-energy information is optimized by maximizing the figure of merit values. The stone materials that are most difficult to separate are calcium oxalate and brushite. The fragility of these materials and ability to fragment them with lithotripsy differs so differentiating these materials is clinically relevant. Therefore for this work the material uses for the figure of merit were calcium oxalate

monohydrate and brushite. CT specifications vary with the manufacturer and model. For the purpose of optimization, the following values were used for all calculations: 0.3 cm slice thickness (s), 0.1 cm detector physical width (w), 1000 detector elements (m), 1000 projections (n), 1 second exposure (1 rotation), and unity detector efficiency (ε). Phantom and stone diameter were set to 20 cm and 1 cm respectively. Inherent CT beam filtration information are normally proprietary, however, conversation with a CT engineer suggests typical values are 1 cm of aluminum and 0.1 cm of titanium so this was used in all calculations. Matlab® (version 2009a, Math-Works, Natick, MA, USA) was used to perform all calculations.

2.3.1 Stone Density

The calculation of F_R^2 and F_N^2 in equation (2.8) and (2.9) can be determined for any spectra and material pair of known composition and density. Measured densities for stone materials were not available so an estimate was calculated based on previous reported CT numbers (10, 17, 27, 28) using:

$$\mu_s = \left(\frac{\mu}{\rho}\right)_s \cdot \rho_s = \mu_w \left(\frac{CT\,\#}{1000} + 1\right) \tag{2.13}$$

where μ_s and μ_w are the linear attenuation coefficients of the stone and water respectively, $(\mu/\rho)_s$ is the mass attenuation coefficient of the stone, and ρ_s is the density of the stone. This equation solves to

$$\rho_s = \rho_w \bullet \frac{\left(\mu/\rho\right)_w}{\left(\mu/\rho\right)_s} \bullet \left(\frac{CT\,\#}{1000} + 1\right) \quad . \tag{2.14}$$

For broad spectra, the effective μ/ρ value is used, equal to an average value weighted by the detected x-ray spectral intensity.

2.3.2 Optimal high and low energy kV and mAs ratio

The figure of merit was calculated for a low energy spectrum ranging from 70 to 100 kVp and a high energy spectrum ranging from 100 to 180. These limits were selected based on the practical lower and upper limit of conventional CT and is consistent with many previous investigations. (7, 9-11, 16, 17, 27, 34) Using the optimal energy combination the figure of merit was calculated using a high-energy mAs of 100, 200 and 300 and an mAs ratio (low energy mAs/ high energy mAs) of 1 to 5 to determine the optimal low and high energy mAs ratio.

2.3.3 Optimal beam-filter material

All possible elements from Z=1 to Z=100, including no filter, were evaluated as possible filter materials. For each, a filter thickness was selected so the incident beam was attenuated by 50%. Additional filtration may have the advantage of further shaping the spectra but also contributes to increased tube loading. A 50% attenuation was selected to explore the benefits of filtration for a modest amount of beam attenuation. It was found that the use of 80% attenuation did not change the selection of the optimal filter materials. The theoretical F_N^2 and F_R^2 was calculated for the stone pair calcium oxalate monohydrate and brushite in a 20 cm water phantom and plotted as a contour plot. Ideal filter selection was made based on filter combinations providing the greatest F_N^2 and F_R^2.

2.4 Results

2.4.1 Optimal high and low energy kV

Figure 2-3 gives the figure of merit over varying energies of the low and high energy spectra assuming a ratio of the low:high energy mAs of 2. Although the value of the figure of merit changes with different mAs ratios the shape of the plot and optimal energy combinations do not differ. For F_N^2 the optimal energy combination is 70 to 73 kVp for the low energy spectrum and 125 to 160 kVp for the high energy spectrum. For F_R^2 70

kVp and 160 to 180 kVp for the low and high energy spectra respectively optimized the figure of merit. These findings support that greater difference in the energies of the dual energy spectra will result in improved results. Until recently the practical lower limit a CT scan is 80 kVp although there are now scanners available that can image at 70kVp. At this value there is minimal additional increase in the figure of merit for energies above 140 kVp for the high energy spectrum therefore this is the energy combination that was evaluated further.

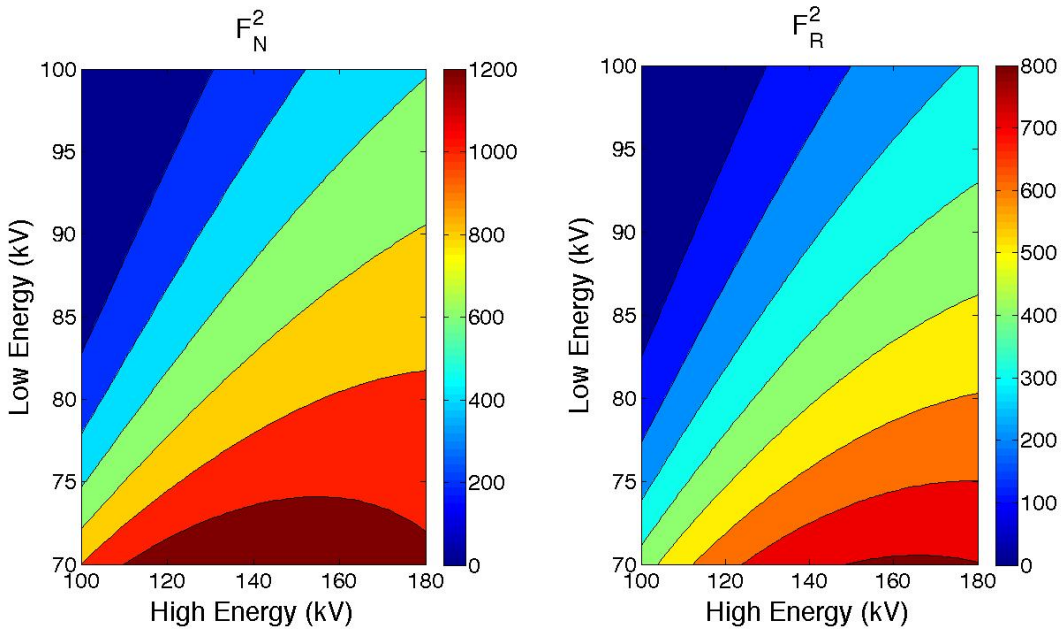

Figure 2-3 Impact of the x-ray energy on the figure of merit for spectra with variable kV of 70 to 100 and 100 to 180 for the low and high energy spectra respectively. For the lowest practical kV of 80 the optimal energy of the high energy spectrum is in the range of 130 to 180 kV but there is minimal increase in the figure of merit above at kV of 140 (stone combination: calcium oxalate monohydrate/brushite).

2.4.2 Stone Density

Average stone density, as estimated from previously published experimental CT numbers, is presented in Table 2-2.(10, 17, 27, 28)

Table 2-2 Stone Density as calculated based on average CT number from previous studies using equation (2.14). The statistical variance in the density measurement represents the variability noted in the previous studies. The effective energy of the 80 kV and 140 kV spectra are 56 keV and 76 keV respectively

Stone	**HU (80 kV)**	**HU (140 kV)**	$\left(\mu/\rho\right)$ **(80 kV)**	$\left(\mu/\rho\right)$ **(140 kV)**	**Density g/cm^2**
Calcium oxalate monohydrate	1244 ± 270	767 ± 120	0.21	0.15	2.26 ± 0.31
Calcium oxalate dihydrate	1346 ± 378	856 ± 210	0.22	0.15	2.21 ± 0.32
Magnesium ammonium phosphate	883 ± 385	637 ± 283	0.25	0.19	1.60 ± 0.30
Hydroxyl apatite	1033 ± 209	670 ± 92	0.57	0.42	0.95 ± 0.03
Brushite	1611 ± 397	1138 ± 319	0.38	0.27	1.47 ± 0.30
Uric acid	377 ± 154	378 ± 140	0.18	0.16	1.60 ± 0.10
Cystine	706 ± 76	549 ± 90	0.26	0.21	1.38 ± 0.09

2.4.3 Optimal mAs Ratio

The optimal mAs ratio was insensitive to beam energy (Figure 2-14) and the maximum improvement in the figure of merit occurred with a mAs ratio of 5 and 3 for F_N^2 and F_R^2 respectively for all energy combinations. However, the broad shape of the mAs ratio curve shows there is latitude in selecting optimal mAs ratio. Therefore a ratio of 2 was used for all subsequent calculations because of the minimal additional impact on the figure of merit and the practicality of clinical use. The figure of merit is independent of

the actual mAs values and dependent only on the mAs ratio. When this calculation was repeated with optimal additional filtration materials the results were unchanged.

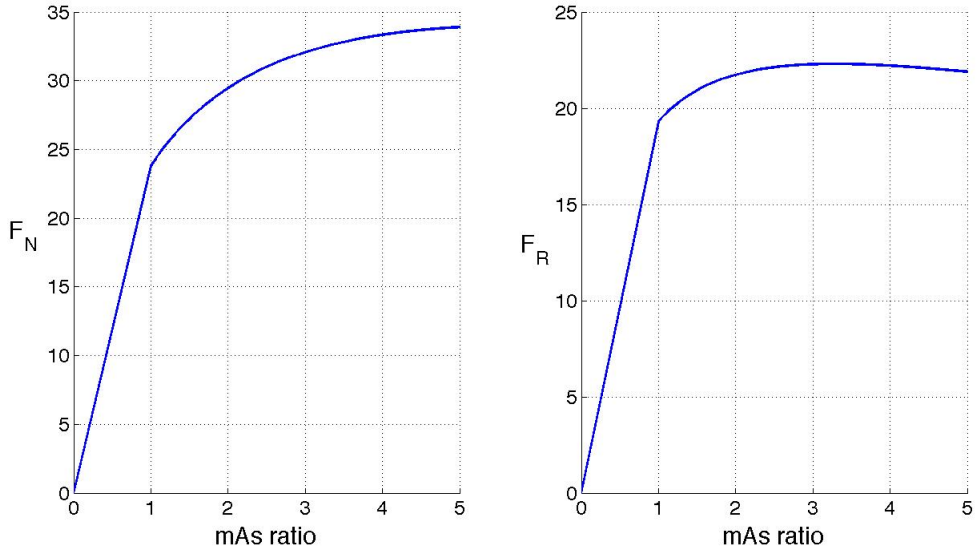

Figure 2-4 Impact of mAs ratio on the square root of the figure of merit (kV 80/140, stone combination: calcium oxalate monohydrate/brushite).

2.4.4 Optimal beam filtration

Optimal beam filtration was selected to give highest F_N^2 and F_R^2. Increasing the mAs of the low energy beam increased the F_N^2 and F_R^2 but the optimal filter materials were the same for all mAs ratios. For both F_N^2 and F_R^2 the maximum separation of the stones occurred with a low energy filter of Z = 66 to 70 and a high energy filter of Z = 44 to 60 (Figure 2-5).

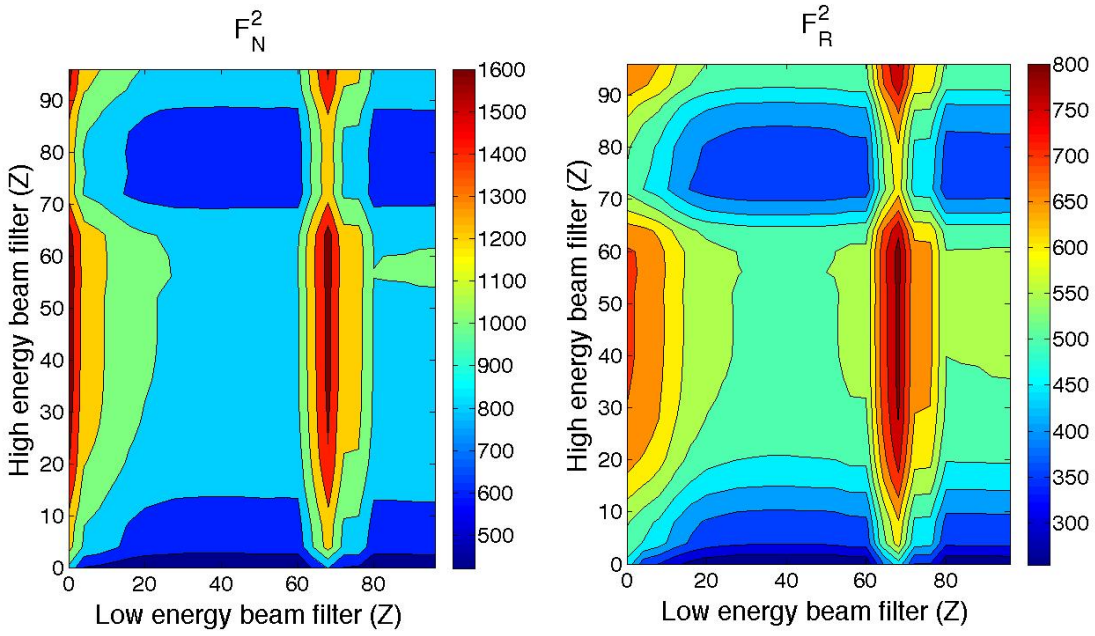

Figure 2-5 Impact of filter high and low energy filter materials on the figure of merit (mAs 200/100, kV 80/140, stone combination: calcium oxalate monohydrate/brushite, filter thickness to attenuate 50% of the primary beam). For both F_R^2 and F_N^2 the maximum separation of the stones occurred with a low energy filter of Z = 66 to 70 and a high energy filter of Z = 44 to 60. Z=0 corresponds to no filter material.

Figure 2-5 shows that applying additional filtration to only the high energy beam also has an impact on the figure of merit. When adding filtration to the high energy there is broad range of materials (Z = 30 to 50) that optimize the figure of merit (Figure 2-5).

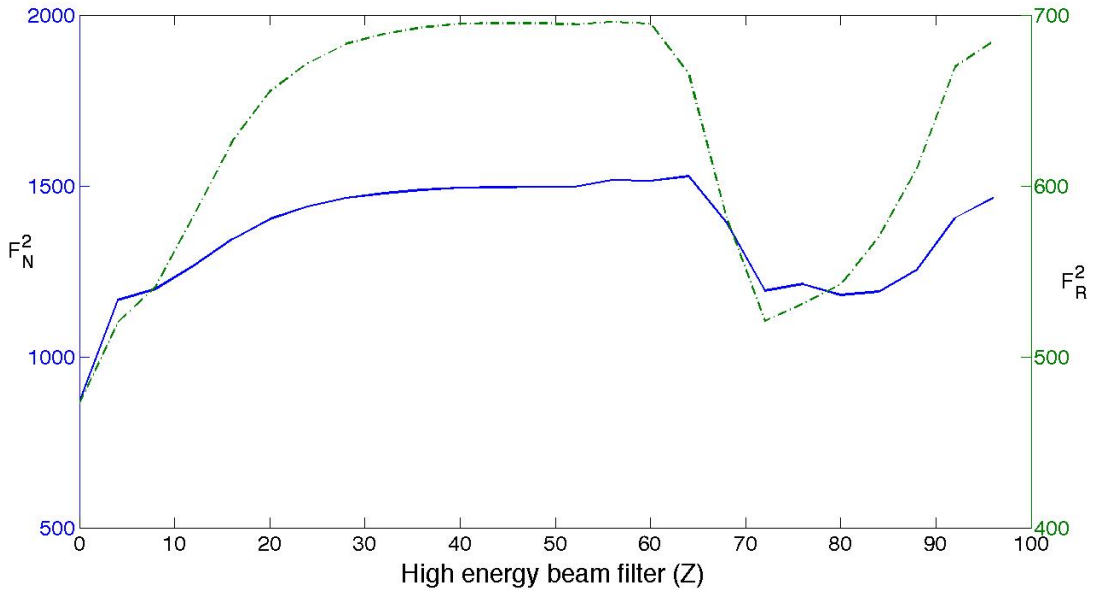

Figure 2-6 Impact filtration of the high energy spectrum only on the figure of merit (mAs 200/100, kV 80/140, stone combination: calcium oxalate monohydrate/brushite)

Based on availability and ease of use a combination of erbium (Z 68) and tin (Z 50) were selected for further evaluation of low and high energy beams respectively as well as filtration of the high energy beam only with tin. Tin (Z 50) was chosen to evaluate further as it is readily available, practical and has been previously noted to improve stone discrimination.(14)

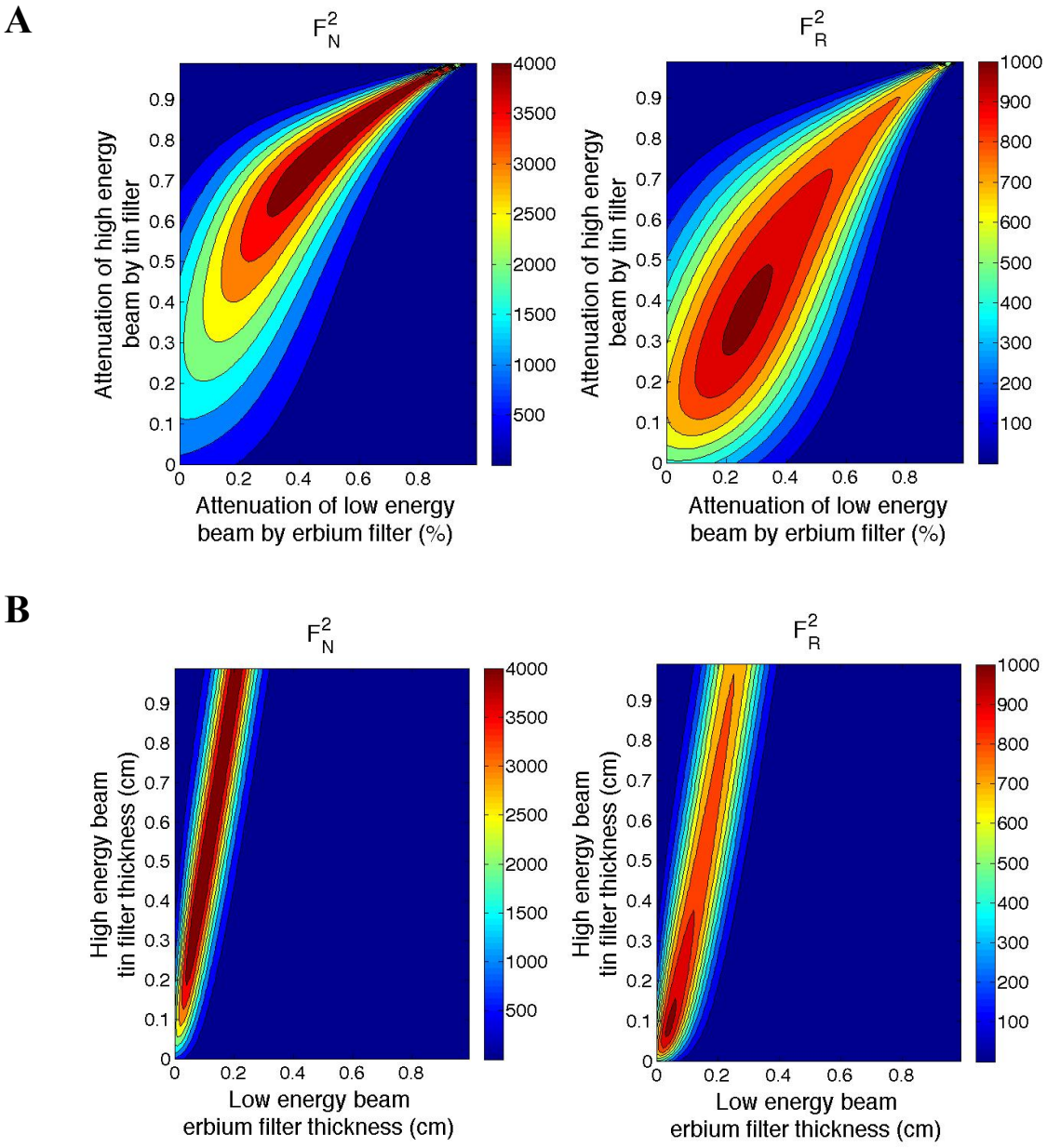

Figure 2-7 Impact of percent beam attenuation (A) and thickness (B) for tin high and erbium low energy filters on the figure of merit (mAs 200/100, kV 80/140, stone combination: calcium oxalate monohydrate/brushite).

Figure 2-7A shows that with an erbium/tin filter combination the optimal F_N^2 and F_R^2 occurred when the attenuation of the low and high energy spectra were 45 and 70%,

respectively. This corresponds to filter thickness of 0.1 cm for erbium and 0.4 cm for tin. Higher levels of attenuation increased the figure of merit but were not considered because of the negative impact of the increasing load on the tube.

A

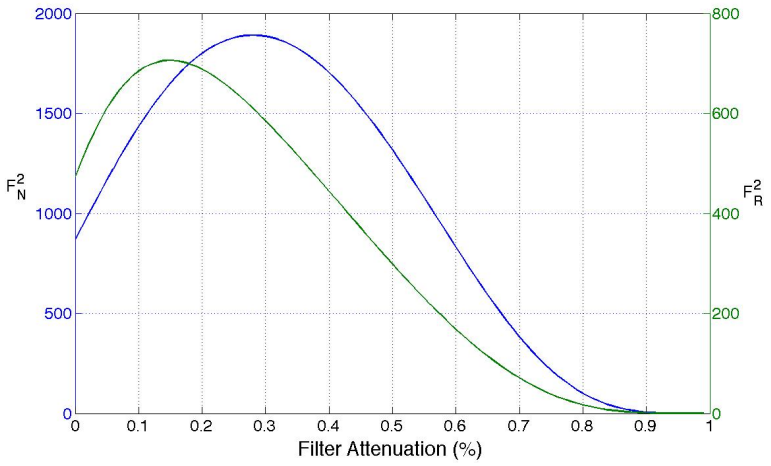

B

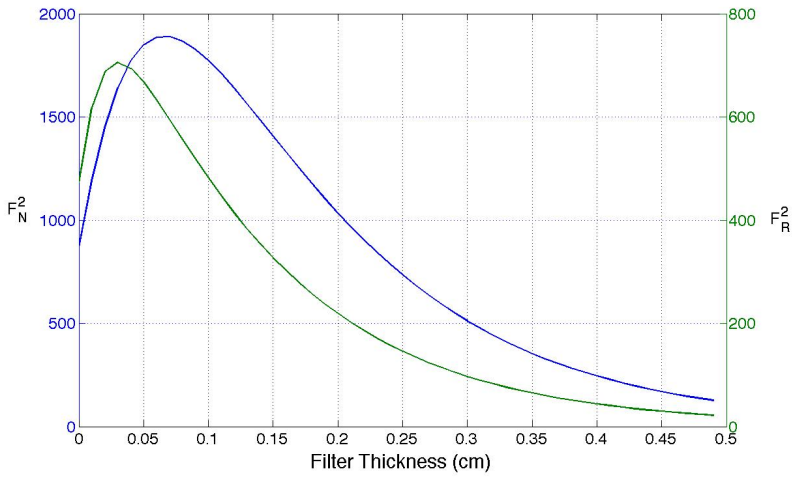

Figure 2-8 Impact of tin high energy filter attenuation (A) and thickness (B) on the figure of merit. Filter thickness is expressed as attenuation of exposure (mAs 200/100, kV 80/140, stone combination: calcium oxalate monohydrate/brushite).

When using a tin high energy filter alone the optimal attenuation was 25% for F_N^2 and 15% F_R^2 for and which corresponds to a 0.06 and 0.03 cm filter thickness respectively.(Figure 2-8) Added filtration has less impact on F_R^2 so a filter thickness of 0.03 to maximize this variable with minimal impact on optimizing F_N^2.

2.4.5 Theoretical stone analysis

For any given measure (dual energy number, dual energy ratio, low energy CT number, high energy CT number) the stones always rank in the same order regardless of the added filtration (Table 2-3).

Table 2-3 Pure stones ranked from lowest to highest dual energy ratio and number (* indicates stones not amenable to shock wave lithotripsy).

Dual energy ratio	**140 kV CT number**	**Dual energy number 80 kV CT number**
Uric acid	Hydroxapatite	Uric acid
Magnesium ammonium phosphate	Uric acid	Cystine*
Cystine*	Cystine*	Magnesium ammonium phosphate
Calcium oxalate	Magnesium ammonium phosphate	Hydroxyapatite
Brushite*	Brushite*	Brushite*
Hydroxyapatite	Calcium oxalate	Calcium oxalate

Table 2-4 shows the figure of merit for the stone combination of calcium oxalate monohydrate/brushite. Both the tin high energy filter and the erbium/tin low/high energy filter combination improved the figure of merit with the combination of an erbium filter of the low energy spectra and tin filter of the high energy spectra resulting in the greatest improvement of the figure of merit. This combination of filter materials resulted in good separation of the energy spectra (Figure 2-9).

Table 2-4 Signal difference to noise ratio per unit dose (F_N^2 and F_R^2) for the stone pair calcium oxalate monohydrate/brushite with a 3 mm^3 voxel using optimal low/high filter combinations and energy settings (200 mAs 80 kV, 100 mAs 140 kV).

Low /High Filter Combination (filter thickness)	F_N^2	F_R^2
None / None	911.9	488.3
None / Tin (0.1 cm)	1726.1	723.9
Erbium (0.1 cm) / Tin (0.4 cm)	3858.4	904.9

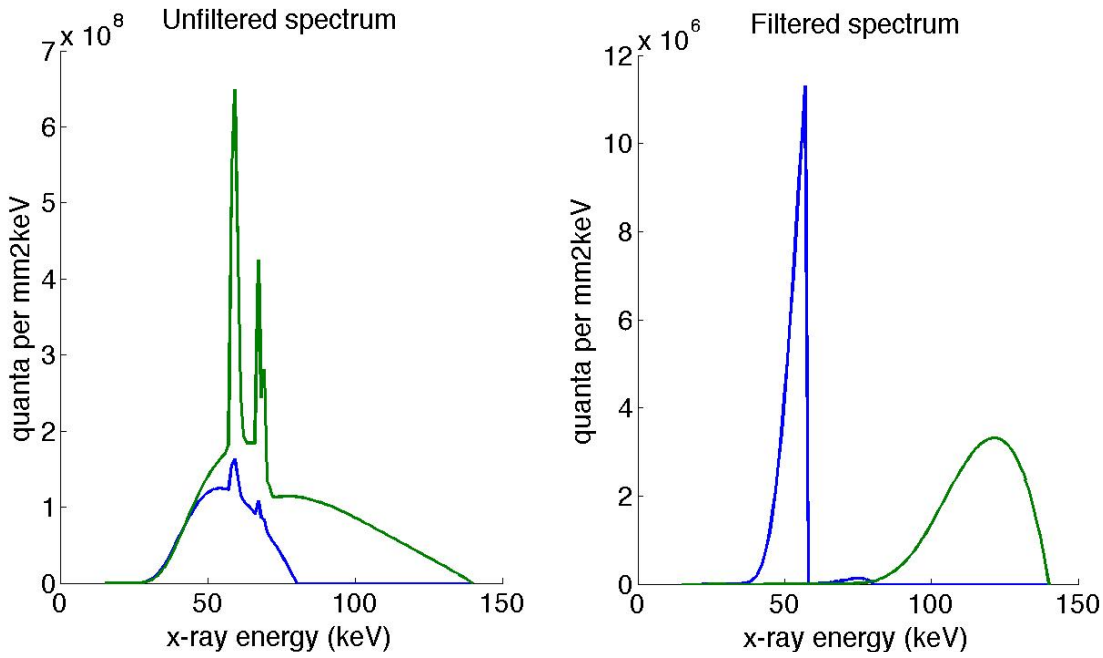

Figure 2-9 Comparison of the unfiltered and filtered spectra demonstrated good spectral separation with filter combination (low energy filter 0.1 cm erbium, high energy filter 0.4 cm tin).

Figure 2-10 and 2-11 shows the Gaussian curves generated from the mean and standard deviation of the dual energy number and dual energy ratio respectively with no task specific filtration. The noise in the dual energy measurement indicates the variance in this theoretical value. The theoretical value +/- 2 standard deviations of the noise will provide a 95% confidence interval in distinguishing between to materials therefore stones that have minimal to no overlap in the noise distribution will be able to be differentiated using the dual energy value. Using this criterion dual energy number is able to differentiate between all stone combinations tested as illustrated by the non-overlapping Gaussian curves in Figure 2-10.

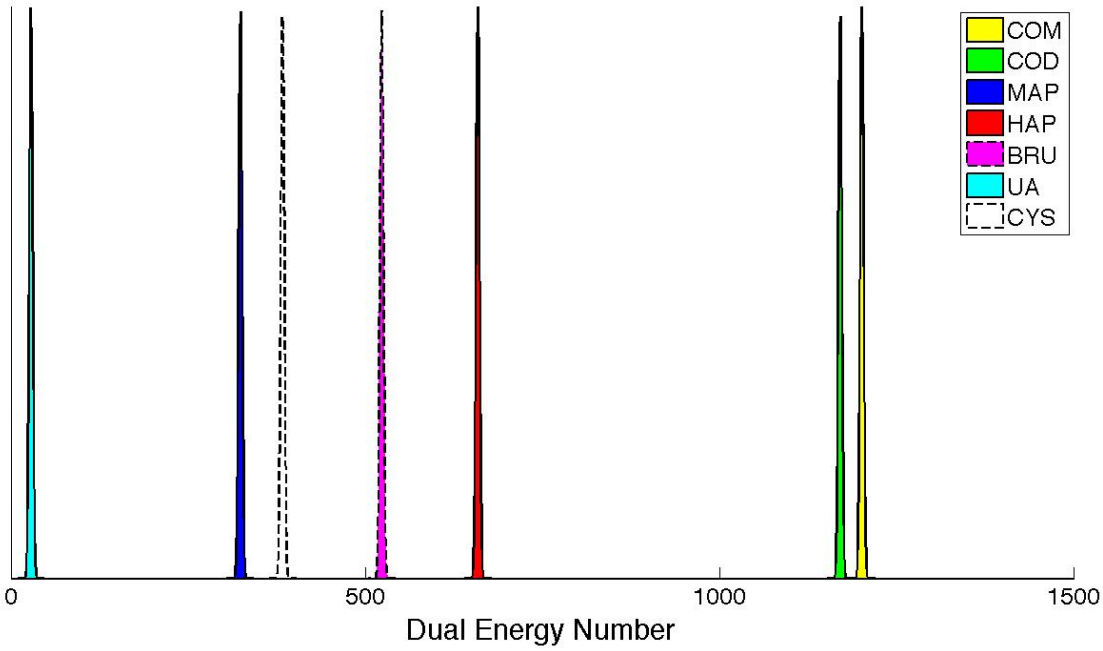

Figure 2-10 Gaussian curves generated from the mean and standard deviation of the dual energy number for pure stone materials. Brushite and cystine are the stone materials that are not amenable to lithotripsy.

Dual energy ratio was slightly less able to differentiate between stone combinations than dual energy number and could not differentiate between calcium oxalate monohydrate and calcium oxalate dihydrate or between cystine and magnesium ammonium phosphate stones (Figure 2-11). We believe the difference between number and ratio is due to the non-linear definition of these values. It is likely they are approximately equal in the limit of small linear attenuation coefficient differences.

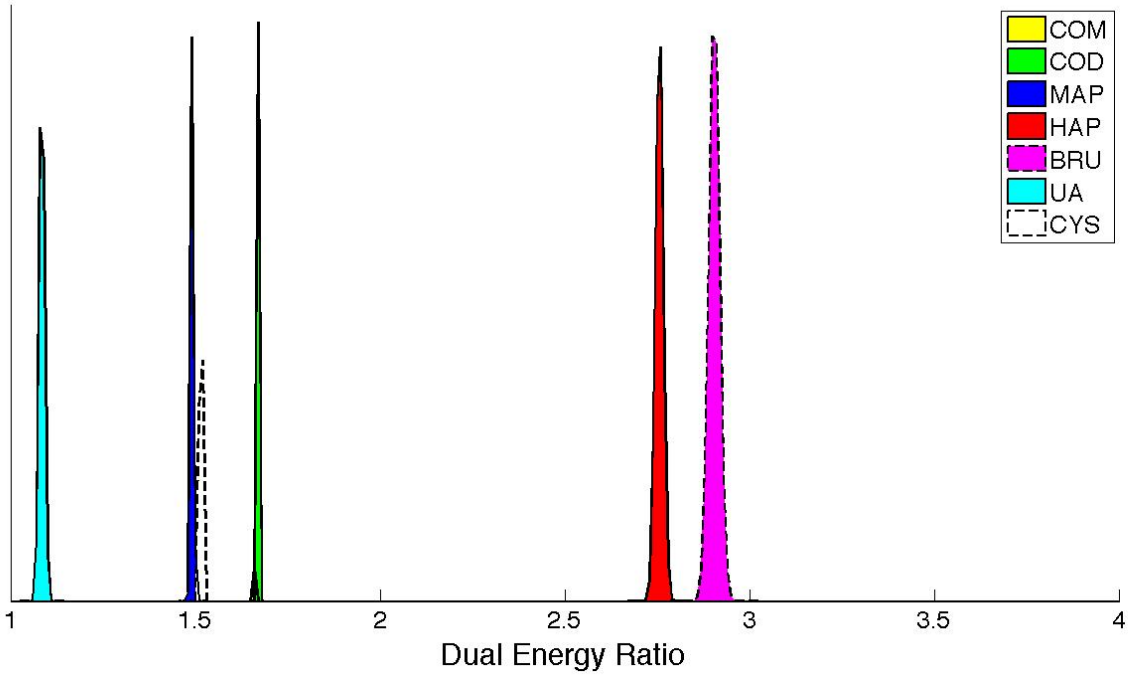

Figure 2-11 Gaussian curves generated from the mean and standard deviation of the dual energy ratio for pure stone materials. Brushite and cystine are the stone materials that are not amenable to lithotripsy. Calcium oxalate stones (monohydrate and dihydrate) have the same distribution.

2.5 Discussion

A figure of merit expressing the difference between the signal to noise ratio of the dual energy number or ratio between two stone materials, normalized to the square-root of the patient average dose, was used to optimized the scan and filter settings for dual energy evaluation of stones. Although this is not a measure that would be used clinically it facilitates a dose-independent comparison of CT settings, filter materials and filter thickness to determine the optimal imaging parameters and determination of whether there is sufficient signal to noise difference to differentiate between two stones.

A single combination of stone materials (brushite/calcium oxalate monohydrate) was used to perform the energy and filter optimization. This combination was selected because differentiating between these stone materials is clinically relevant. An alternative would have been to test the stone pair with the greatest difference in figure of merit values (hydroxyapatite/uric acid). Although the absolute CT numbers, and subsequently the S_N and S_R, are dependent on filter material, beam energy combination and mAs ratio, the rank order of CT number, S_N, and S_R for pure composition stones is independent of these parameters. Therefore, by increasing the spread of the dual energy values the probability that stones can be distinguished from each other is increased regardless of the stone combination.

Using the figure of merit the optimal CT parameters were determined to be 80 and 140 kVp for the low and high energy spectra which is consistent with parameters used in previous studies.(2-15) To compensate for loss of signal with the low energy spectra due to greater attenuation the mAs of the scan would need to be increased to ensure an acceptable noise in the image. The optimal ratio of the mAs of the low and high energy beams was 5 and 3 for F_N^2 and F_R^2 but there was only a small increase in the figure of merit with a ratio of greater than 2 in both cases. Therefore, given the importance of minimizing patient dose, a ratio of greater than 2 is not recommended.

The most accurate method for material discrimination with dual energy imaging is using two monoenergetic beams.(20, 21) In the case of a spectrum there is a broad distribution of energies in the beam, which results in overlap of energies between spectra of two

different energies. The addition of filter materials in the path of the beam will change the shape of the spectrum and result in less overlap of energies between the two beams. This results in a closer approximation of the monoenergetic case and improves the ability to discriminate between materials. The second objective of this study was to determine whether the addition of filtration to the low and high energy spectra would result in improvement in the figure of merit. Although the figure of merit was evaluated over all materials and thicknesses the ultimate choice of filter must also consider practicality of use and availability. Given these constraints the filter combination that optimized the figure of merit was a 0.1 cm erbium filter and a 0.4 cm tin filter for the low and high spectra respectively. When comparing the unfiltered spectrum the spectrum filtered with this combination of materials it is evident that there is clear separation of the dual energy spectra in the filtered case and that explains the approximately two to four-fold improvement in the figure of merit for F_R^2 and F_N^2 respectively.

Numerous authors have presented varied results on dual energy CT and the ability to discriminate stone types with both dual energy number and dual energy ratio.(3, 10, 17, 35, 36) One possibility for these varied results is that there is insufficient signal difference to noise to discriminate between the stone materials. However, this work has shown that in a theoretical model there is sufficient signal difference to noise for the dual energy number. This work was done using a pure composition stone. Pure stones are uncommon in clinical practice and previous studies have had varied criteria for defining a pure stone and most range from 70-80% of a single stone material. This variation in purity is likely a major contributing factor to the varied results in the in vivo clinical determination of stone material. Most stones have a central nidus and circumferential layers of various stone materials which can be readily demonstrated with coherent scatter CT and on visual inspection.(37) A previous study indicated that various materials could be differentiated within a single stone however the distribution of the material was linear across the entire diameter of the stone.(35) This distribution of material has not been reported previously therefore this may represent an imaging artifact rather than true differentiation of layering of stone materials. It is possible that even though dual energy number can theoretically discriminate between pure stone materials the inherent variation in stone purity noted clinically cannot be overcome with dual energy imaging.

Although additional beam filtration can improve material discrimination has historically been difficult to add to the CT scanners; however, newer dual source CT scanners do permit the addition of filtration to one or both x-ray sources so it is important to determine if there is sufficient signal difference to noise with the unfiltered spectra and whether the addition of beam filtration results in the ability to discriminate between clinically important stone materials that could not be differentiated with the unfiltered spectra. The dual energy number had a greater ability to differentiate between stone pairs than the dual energy ratio and could differentiate between all stone combinations even in the absence of additional beam filtration. Both dual energy number and dual energy ratio have been evaluated for determination of stone composition. In one study dual energy ratio was reported as able to differentiate between all stone types (10) while in another could only differentiate calcium containing from other stones.(35, 36) Dual energy number has had similar mixed results from being able to differentiate all stones (3) and to only differentiating select combinations (17). From this theoretical model it can be concluded that the dual energy number is more likely to be able to discriminate between stone materials without the need for task specific filtration but task specific filtration may be advantageous in overcoming challenges with mixed composition stones and should be further evaluated in that scenario.

2.6 Conclusions

There is fundamentally sufficient signal to noise difference between clinically relevant stone materials to allow for differentiation using dual energy number for an acceptable voxel size and patient dose using the dual energy number but not the dual energy ratio. Because all pure stone materials can be differentiated with the dual energy number t is difficult to justify the engineering and implementation costs to add task specific filtration to a CT scanner. However, given there is sufficient signal to noise difference to differentiate pure stones and yet clinically the results are highly varied, the added ability to discriminate stones provided by the use of added filtration may be important in the clinical scenario of mixed composition stones. Given the mixed purity noted in clinical stones perhaps the clinically relevant question is not the stone composition but rather

whether a stone is amenable to shockwave lithotripsy or not. Dual energy CT may provide more consistent results in evaluating this question than that of stone material.

References:

1. Trinchieri A. Epidemiological trends in urolithiasis: impact on our health care systems. Urol Res. 2006;34(2):151-6.

2. Demirel A, Suma S. The efficacy of non-contrast helical computed tomography in the prediction of urinary stone composition in vivo. J Int Med Res. 2003;31(1):1-5.

3. Mostafavi MR, Ernst RD, Saltzman B. Accurate determination of chemical composition of urinary calculi by spiral computerized tomography. J Urol. 1998;159(3):673-5.

4. Mitcheson HD, Zamenhof RG, Bankoff MS, Prien EL. Determination of the chemical composition of urinary calculi by computerized tomography. J Urol. 1983;130(4):814-9.

5. Hillman BJ, Drach GW, Tracey P, Gaines JA. Computed tomographic analysis of renal calculi. AJR Am J Roentgenol. 1984;142(3):549-52.

6. Hidas G, Eliahou R, Duvdevani M, et al. Determination of renal stone composition with dual-energy CT: in vivo analysis and comparison with x-ray diffraction. Radiology. 2010;257(2):394-401.

7. Thomas C, Patschan O, Ketelsen D, et al. Dual-energy CT for the characterization of urinary calculi: In vitro and in vivo evaluation of a low-dose scanning protocol. Eur Radiol. 2009;19(6):1553-9.

8. Thomas C, Heuschmid M, Schilling D, et al. Urinary calculi composed of uric acid, cystine, and mineral salts: differentiation with dual-energy CT at a radiation dose comparable to that of intravenous pyelography. Radiology. United States: Rsna, 2010., 2010; p. 402-9.

9. Graser A, Johnson TR, Bader M, et al. Dual energy CT characterization of urinary calculi: initial in vitro and clinical experience. Invest Radiol. 2008;43(2):112-9.

10. Boll DT, Patil NA, Paulson EK, et al. Renal stone assessment with dual-energy multidetector CT and advanced postprocessing techniques: improved characterization of renal stone composition--pilot study. Radiology. 2009;250(3):813-20.

11. Primak AN, Fletcher JG, Vrtiska TJ, et al. Noninvasive differentiation of uric acid versus non-uric acid kidney stones using dual-energy CT. Acad Radiol. 2007;14(12):1441-7.

12. Saw KC, McAteer JA, Monga AG, Chua GT, Lingeman JE, Williams JC, Jr. Helical CT of urinary calculi: effect of stone composition, stone size, and scan collimation. AJR Am J Roentgenol. 2000;175(2):329-32.

13. Qu M, Jaramillo-Alvarez G, Ramirez-Giraldo JC, et al. Urinary stone differentiation in patients with large body size using dual-energy dual-source computed tomography. Eur Radiol. 2013;23(5):1408-14.

14. Qu M, Ramirez-Giraldo JC, Leng S, et al. Dual-energy dual-source CT with additional spectral filtration can improve the differentiation of non-uric acid renal stones: an ex vivo phantom study. AJR Am J Roentgenol. 2011;196(6):1279-87.

15. Wang J, Qu M, Duan X, et al. Characterisation of urinary stones in the presence of iodinated contrast medium using dual-energy CT: a phantom study. Eur Radiol. 2012;22(12):2589-96.

16. Thomas C, Heuschmid M, Schilling D, et al. Urinary calculi composed of uric acid, cystine, and mineral salts: differentiation with dual-energy CT at a radiation dose comparable to that of intravenous pyelography. Radiology. 2010;257(2):402-9.

17. Matlaga BR, Kawamoto S, Fishman E. Dual source computed tomography: a novel technique to determine stone composition. Urology. 2008;72(5):1164-8.

18. Gauntt DM, Barnes GT. X-ray tube potential, filtration, and detector considerations in dual-energy chest radiography. Med Phys. 1994;21(2):203-18.

19. Boone JM, Shaber GS, Tecotzky M. Dual-energy mammography: a detector analysis. Med Phys. 1990;17(4):665-75.

20. Primak AN, Ramirez Giraldo JC, Liu X, Yu L, McCollough CH. Improved dual-energy material discrimination for dual-source CT by means of additional spectral filtration. Med Phys. 2009;36(4):1359-69.

21. Richard S, Siewerdsen JH. Optimization of dual-energy imaging systems using generalized NEQ and imaging task. Med Phys. 2007;34(1):127-39.

22. Bushberg J. The essential physics of medical imaging: Lippincott Williams & Wilkins, 2012.

23. Faulkner K, Moores BM. Noise and contrast detection in computed tomography images. Phys Med Biol. 1984;29(4):329-39.

24. Holdsworth DW, Drangova M, Fenster A. A high-resolution XRII-based quantitative volume CT scanner. Medical physics. 1993;20(2 Pt 1):449-62.

25. Brooks RA, Di Chiro G. Statistical limitations in x-ray reconstructive tomography. Med Phys. 1976;3(4):237-40.

26. El-Assmy A, Abou-El-Ghar ME, El-Nahas AR, Refaie HF, Sheir KZ. Multidetector Computed Tomography: Role in Determination of Urinary Stones Composition and Disintegration With Extracorporeal Shock Wave Lithotripsy-an in Vitro Study. Urology: 2010 Elsevier Inc, 2010.

27. Bellin MF, Renard-Penna R, Conort P, et al. Helical CT evaluation of the chemical composition of urinary tract calculi with a discriminant analysis of CT-attenuation values and density. Eur Radiol. 2004;14(11):2134-40.

28. Grosjean R, Sauer B, Guerra RM, et al. Characterization of human renal stones with MDCT: advantage of dual energy and limitations due to respiratory motion. AJR Am J Roentgenol. 2008;190(3):720-8.

29. Huda W, Ogden KM, Lavallee RL, Roskopf ML, Scalzetti EM. In-patient to isocenter KERMA ratios in CT. Med Phys. 2011;38(10):5362-9.

30. Johns HE, Cunningham JR. The Physics of Radiology. Springfield, IL: Charles C Thomas, 1983.

31. Huda W. Medical radiation dosimetry. RSNA categorical course in diagnostic radiology physics: from invisible to visible - the science and practice of x-ray imaging and radiation dose optimization. Oak Brook, IL: RSNA, 2006; p. 29-39.

32. Mathieu KB, McNitt-Gray MF, Zhang D, Kim HJ, Cody DD. Precision of dosimetry-related measurements obtained on current multidetector computed tomography scanners. Med Phys. 2010;37(8):4102-9.

33. Prien EL, Prien EL. Composition and structure of urinary stone. The American journal of medicine. 1968;45(5):654-72.

34. Zilberman DE, Ferrandino MN, Preminger GM, Paulson EK, Lipkin ME, Boll DT. In vivo determination of urinary stone composition using dual energy computerized tomography with advanced post-acquisition processing. J Urol. 2010;184(6):2354-9.

35. Graser A, Johnson TRC, Bader M, et al. Dual energy CT characterization of urinary calculi: initial in vitro and clinical experience. Invest Radiol. 2008;43(2):112-9.

36. Thomas C, Heuschmid M, Schilling D, Ketelsen D. Urinary Calculi Composed of Uric Acid, Cystine, and Mineral Salts: Differentiation with Dual-Energy CT at a Radiation Dose Comparable to That of Intravenous Pyelography. Radiology. 2010;257(2):402-9.

37. Wignall GR, Cunningham IA, Denstedt JD. Coherent scatter computed tomography for structural and compositional stone analysis: a prospective comparison with infrared spectroscopy. J Endourol. 2009;23(3):351-7.

Chapter 3 - Dual energy computed tomography of canine urinary calculi

This chapter will be submitted to Veterinary Radiology and Ultrasound

Urolithiasis is a common problem in veterinary medicine. In dogs and cats magnesium ammonium phosphate (struvite) and calcium oxalate stones are the most common stone type with an incidence of 39-53% and 35-45% respectively.(1-3) Urate stones are also common accounting for approximately 24% of stones submitted for analysis.(2) Although the overall incidence of urolithiasis has not changed dramatically over the past several decades there has been a dramatic shift in the type of stones identified with a decrease in struvite stones and an increase in calcium oxalate stones. This is thought to be due to improvements in the dietary management of struvite stones. It is also theorized that diets that manage struvite stones increase the risk of developing calcium oxalate stones.(1-3)

Cystic calculi are easily treated with surgery but there are higher complication rates with surgical treatment of renal and ureteral calculi. Both extracorporeal and intracorporeal shock wave lithotripsy are being used with increasing frequency for the treatment of cystic and renal or ureteral calculi respectively. However, extracorporal shock wave lithotripsy (ESWL) is not without side effects including hypertension, loss of renal function, and an increase in stone recurrence.(4) Not all stones are amenable to fragmentation with ESWL, with failure rates of 9.4 to 26.3% reported in people and the probability of success of shock wave lithotripsy is dependent on the stone composition.(5, 6) It is generally considered that calcium oxalate, struvite and hydroxyapatite stones are amenable to ESWL while brushite and cystine stones are not.(7-9) Uric acid stones are also amenable to ESWL but are also amenable to medical management and can be dissolved with dietary management if they are non obstructive. Considering both the

potential risks and the costs it is clear that an in vivo method (currently unavailable) to determine stone composition would be advantageous to facilitate optimal treatment selection.

Dual energy imaging exploits the differences in the differences in the probability of the photoelectric and Compton interactions and the variability of k-edges between various tissues.(10-12) This results in the relative linear attenuation coefficients being different at different energies (Figure 3-1). Images are acquired at both a high and low kV and the image data is combined into a dual energy measurement. Although dual energy CT scanners that can acquire this data in a single scan are available they are not required to perform this test and measurements from two consecutively acquired scans can be used to calculate the dual energy value. The most common dual energy measurements are the dual energy number (low energy CT# - high energy CT#) and the dual energy ratio (low energy CT# ÷ high energy CT#).

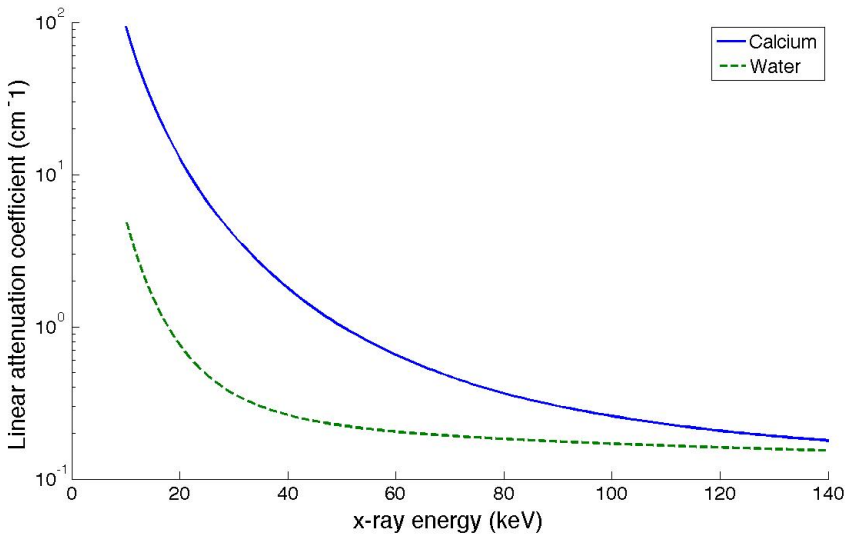

Figure 3-1 Linear attenuation coefficients of water and calcium from 10 to 120 kV. At a given energy the relative difference in linear attenuation coefficients is different. This difference is exploited in dual energy measurements to determine material composition

Dual energy measurements to determine stone composition in vivo have been evaluated in people with varied success.(13-23) This variability may be due to different imaging parameters, variability in the purity of the stones, and measurement of artifact. Previous work by our group has established the optimal imaging parameters for dual energy scanning of urinary calculi.

The objective of this study is to determine whether the dual energy number and ratio of canine stones in a phantom model is able to differentiate stone materials.

3.1 Materials and Methods

Thirty bladder stones from the canine urolithiasis bank previously determined to be greater than 70% pure composition were evaluated with dual energy CT. Stones were suspended in the centre of a 16 cm diameter phantom made of agar.(Figure 3-2) A GE 64 slice dual energy CT scanner was used for all studies. Two scans were acquired using 140 kV and 100 mAs and 80 kV and 100 mAs with a 50 cm scan field of view. All series used an axial scan with a slice thickness of 0.625 mm and an abdomen (soft tissue) reprocessing algorithm.

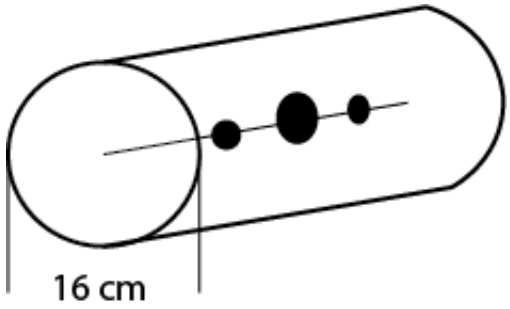

Figure 3-2 Schematic of the CT phantom. Stones were suspended in the centre of the agar phantom.

A manual region of interest was drawn around the stone excluding the visible partial volume artifact along the periphery to obtain the average CT number. This was performed a total of three times. A computer generated ROI was drawn for each stone using a threshold value that included the entire stone. The dual energy number (low energy CT # – high energy CT #) and dual energy ratio (low energy CT # ÷ high energy CT #) was calculated for each stone. High and low energy CT numbers were also recorded. Agreement between the manual regions of interest and threshold region of interest was determined by linear regression and concordance correlation. A Bland-Altman test with a student t-test on the differences was used to assess the variability in the measures. The gold standard for stone composition was determined with standard laboratory analysis performed by the Urolithiasis center in Guelph, Ontario. Data from one manual region of interest and the computer generated threshold region of interest were assessed for normality and compared using an ANOVA with significance set at 0.05. A Tukey-Kramer adjustment was made to reduce type one error.

3.2 Results

The thirty stones were comprised of brushite (3), calcium oxalate (4), cystine (5), struvite (10), and urate (8). A bias existed to struvite and urate stones because of an attempt to select near pure composition stones. In dogs urate stones form due to metabolic changes and are most likely to be of pure composition. Struvite stones form secondary to infection increasing the incidence of occurrence. Stones ranged in size from 1 to 40 mm in diameter.

For all four measures agreement between the 3 manually drawn and the threshold region of interest was excellent with a correlation of $r > 0.95$ for all comparisons (Figure 3-3). No significant bias was detected.

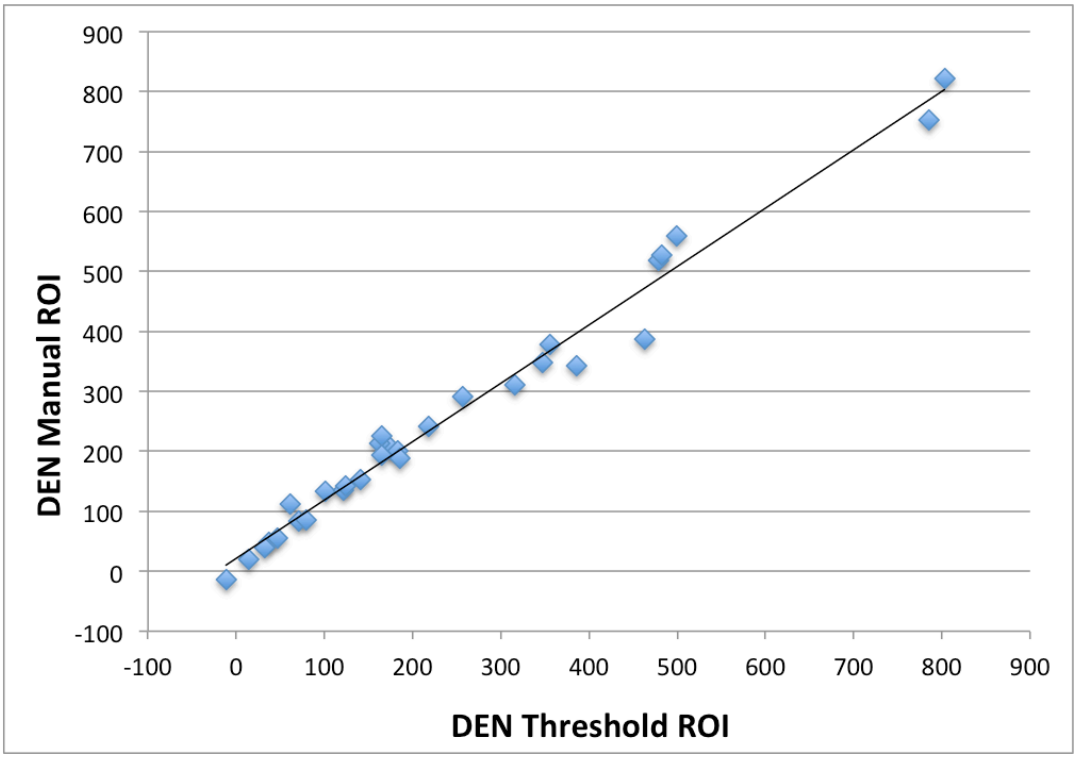

Figure 3-3 Agreement between the manual drawn region of interest and the threshold region of interest for the dual energy number

Figure 3-4 shows CT images of a struvite stone obtained at 80 and 140 kV. At 80 kV the inhomogeneity of the stone material is more evident.

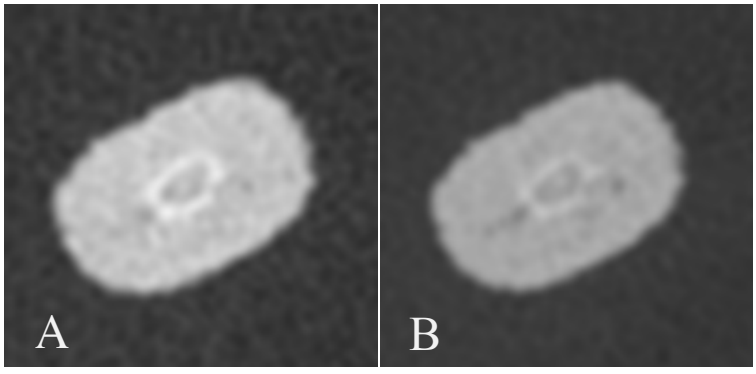

Figure 3-4 CT image of a struvite stone at 80 kV(A) and 140 kV (B)

The dual energy ratio and number and high and low energy CT values for the various stones is given in Table 3-1. All data sets were normally distributed. Manual and threshold regions of interest showed the same significant differences.

Table 3-1 Dual energy ratio, dual energy number and high and low energy CT numbers for stone types (mean +/- standard error) using the manual region of interest

Stone	High CT#	Low CT#	Dual Energy Ratio	Dual Energy Number
Struvite	797 ± 62	1050 ± 87	1.31 ± 0.02	253 ± 29
Calcium Oxalate	1093± 98	1584 ± 138	1.45 ± 0.04	491 ± 46
Cystine	506 ± 88	668 ± 124	1.33 ± 0.03	162 ± 41
Urate	496 ± 69	550 ± 98	1.09 ± 0.03	54 ± 33
Brushite	1403 ± 98	2012± 160	1.43 ± 0.04	609 ± 53

Significant differences in the pairwise comparisons for dual energy number and dual energy ratio are given in Table 3-2. No single measure differentiated between all stone types. Dual energy ratio is only able to differentiate urate stones from the other types and calcium oxalate from struvite. Dual energy number can differentiate struvite from calcium oxalate, urate from calcium oxalate, and urate and struvite; calcium oxalate from cysteine, cystine and brushite; and urate from brushite. The low energy CT number was able to differentiate struvite from calcium oxalate, urate and struvite, struvite and brushite, calcium oxalate from cysteine, urate and calcium oxalate, urate and brushite; and cysteine from brushite. If all three measures (dual energy ratio, dual energy number and low CT number) are used then all stones can be differentiated except for struvite and cysteine.

Table 3-2 Significant differences in the pair wise comparisons dual energy ratio (♦), dual energy number (X) and low energy CT number (*). Cystine and brushite stones are not amenable to shockwave lithotripsy.

STONE	Struvite	Calcium Oxalate	Urate	Cystine	Brushite
Struvite		♦ X *	♦ X *		X *
Calcium Oxalate			♦ X *	X *	
Urate				♦	♦X *
Cystine					X *
Brushite					

Based on reported fragility of stones cystine and brushite are not amenable to shock wave lithotripsy so differentiating these from the other stone materials in vivo would enable appropriate treatment selection.(7, 8, 24, 25) Cystine can only be differentiated from calcium oxalate with the dual energy number and low energy CT number, and from urate with the dual energy ratio. Cystine could not be differentiated from struvite. Brushite could be differentiated from all materials except calcium oxalate using both dual energy number and low energy CT number.

3.3 Discussion

With the increasing availability of both intracorporeal and extracorporeal shock wave lithotripsy and the variable effectiveness of these techniques in fragmenting stones depending on the stone composition an in vitro method of determining stone composition would be advantageous to guide appropriate treatment selection and decrease patient morbidity.

CT attenuation values are related to the density of the material in a non-linear manner. A single energy technique to obtain CT attenuation values for stones initially showed

promise in vivo but subsequent in vitro work showed poor reproducibility and too much overlap between stone types to be useful.(14, 18, 25-27) Partial volume averaging with the surrounding soft tissues confound in vitro use of simple linear attenuation values making them less accurate. With wider collimation and higher pitch the density of the stone may be artificially reduced by the inclusion of the surrounding soft tissue in the measurement.(28) This may explain differences noted between in vivo and in vitro studies as in the in vivo studies tend to have thinner collimation.(13) Saw et. al showed that this effect can be corrected for using a mathematical model described by Hu and Fox but is now less of a problem with the increasing use of multi-slice scanners capable of sub millimeter collimation.(28) Currently most physicians accept that single energy CT measurements can only differentiate uric acid stones from others.(29)

In this experimental model dual energy ratio, dual energy number, or the CT number from the low energy scan were insufficient as single measurements to differentiate between the different stone types. However, when using all three measures together all stones can be differentiated with the exception of struvite and cystine. The differentiation of struvite and cystine stones can be made based on other diagnostic testing so the inability of dual energy CT to differentiate these stones is not clinically relevant.

Dual energy CT has been used to determine urinary stone composition in humans with varying success. Potential reasons for the marked variability in the DECT results could include errors in the CT measurements due to beam hardening artifact, partial volume averaging, misregistration of the dual energy images (due to patient motion between images), and CT scanner calibration errors. Partial volume averaging should not affect dual energy calculations as both the high and low energy measurements will be affected in a similar manner.(22) However, in small stones partial volume averaging may result in incorrect material characterization even with dual energy imaging because of inaccurate measurement of stone density. Misregistration of the images was a potential source of error in the early work because the technology did not exist to acquire the images nearly simultaneously. Images were either acquired in two consecutive scans at different energies or alternating slices were acquired at different energies so the images were offset by the slice thickness. Dual energy CT scanners that can acquire images nearly

simultaneously are now available so this is less likely to be a source of error in more recent studies.

Another possible explanation for the inability to differentiate stone materials is the linear attenuation coefficient is dependent on the density of the material and the density of stones may be independent of the stone composition so variations in density may be sufficiently great that there is overlap between stones of varied composition. The dual energy ratio should be independent of the density because the numerator and denominator are equally affected by the density of the material but the energy of the beam affects the degree of beam hardening so a higher density material may have more beam hardening with the low energy scan than the high energy scan resulting in an unequal effect on values in the ratio.

An additional consideration is that many stones are not purely composed of one material. Testing of stones can be done using polarized light microscopy, infrared spectroscopy and x-ray diffraction techniques. All of these methods are destructive and test only portions of the stone. When distinct layering is noted in a stone all layers are evaluated but if no clear layering is present only a single representative sample may be tested. Infrared spectroscopy uses light to stimulate atomic vibration resulting in energy absorption. The pattern of absorption bands can be compared to standards of pure samples to determine the composition. Mixed samples can also be evaluated, as the mixed spectrums are a simple overlay of the individual pure spectrums.(30, 31) This analysis can examine small samples, can detect the non crystalline components (fat or protein) and can be semi-automated.(32) Currently Fourier transform infrared spectroscopy (FTIR) and attenuated total internal reflection Fourier transform infrared spectroscopy (ATR-FTIR) are used for stone analysis. ATR-FTIR has the advantage of requiring less sample preparation. Measurements are independent of sample thickness so less grinding is required and ATR does not require mixing the sample with an infrared inactive material.(32, 33) X-ray diffraction methods involve radiating a powdered sample with a monoenergetic beam. The x-rays are diffracted by the sample in a characteristic pattern. This provides a very robust method of accurately identifying the composition of stones and quantitate the components and is considered to be the gold standard in clinical

stone analysis but is limited by the sample size.(34, 35) It was shown than in mixed stones if less than 5-15% of a compound was present it would not be detected with x-ray diffraction.(30, 32, 36) As a result stones that are reported as pure composition may have 5 to 10% of another material present that would alter the CT values. These sources of variability may contribute the failure of dual energy CT to provide adequate material discrimination.

The primary reason for an in vivo test for stone composition is to predict whether a stone can be broken with shock wave lithotripsy. As a result there has been considerable interest in developing in vivo assessments of stone composition and correlating stone composition with fragility and to allow for appropriate treatment decisions. Numerous authors have reported experiences with shockwave lithotripsy and stone fragility. Uric acid stones are known for being soft and easily fragmented with shock wave therapy while brushite and cystine stones are harder and as a result are resistant to ESWL.(7, 9, 37) Struvite, uric acid and calcium oxalate dihydrate stones tend to fragment into small pieces while calcium oxalate monohydrate tends to fragment into larger pieces that are less likely to pass.(38) It has also been shown that within a specific chemical composition (particularly calcium oxalate monohydrate stones) there is great variability in stone fragility (co-efficient of variability 60%).(37) The reason for this variability is poorly understood but may be related to variations in minor chemical elements or the presence of a central core of a different composition.(29) Within calcium oxalate monohydrate stones the concentration of magnesium, manganese and zinc were significantly lower in stones that were successfully fragmented with ESWL versus those that failed treatment.(38) Adams et. al. compared the fragility of calcium monohydrate stones from dogs and cats and found that feline stones were harder to break than canine stones in spite of the same chemical composition.(39) This may be due to varying amounts of organic material or a mix of minerals being present.(37) Mandhani et. al. used dual x-ray absorptiometry (DXA) to assess stone fragility and determined that fragility was correlated to stone mineral content and not mineral density. They hypothesized that a classification scheme that is independent of composition and based on stone mineral content would answer the clinically relevant question of whether stones can be fragmented with ESWL or not.(40) This has also been demonstrated with CT attenuation

where the higher the attenuation, regardless of the composition, the less likely the stone can be fragmented with ESWL.(25) Stone composition is important in treatment planning but stone site, stone size, stone number, history of urolithiasis, hydronephrosis, renal colic, and ureteral stents also affect the success rate of ESWL.(24, 41)

3.4 Conclusions

There is no single CT measurement that can be used to differentiate between struvite, calcium oxalate, cystine, urate and brushite stones. Given the lack of discrimination of stone type with dual energy CT, and that the primary reason for determining stone composition in vivo is to predict response to shock wave lithotripsy, it would be beneficial for future work to correlate dual energy values to stone fragility rather than stone type.

References:

1. Houston DM, Moore AE. Canine and feline urolithiasis: examination of over 50 000 urolith submissions to the Canadian veterinary urolith centre from 1998 to 2008. Can Vet J. 2009;50(12):1263-8.

2. Low WW, Uhl JM, Kass PH, Ruby AL, Westropp JL. Evaluation of trends in urolith composition and characteristics of dogs with urolithiasis: 25,499 cases (1985-2006). J Am Vet Med Assoc. 2010;236(2):193-200.

3. Ettinger S, Feldman E. Textbook of Veterinary Internal Medicine: Elsevier - Health Sciences Division, 2004.

4. Stoller M, Meng M. Urinary stone disease: the practical guide to medical and surgical management. Towata, New Jersey: Humana Press, 2007.

5. Logarakis NF, Jewett MA, Luymes J, Honey RJ. Variation in clinical outcome following shock wave lithotripsy. J Urol. 2000;163(3):721-5.

6. Ehreth JT, Drach GW, Arnett ML, et al. Extracorporeal shock wave lithotripsy: multicenter study of kidney and upper ureter versus middle and lower ureter treatments. J Urol. 1994;152(5 Pt 1):1379-85.

7. Evan AP, Coe FL, Lingeman JE, Worcester E. Insights on the pathology of kidney stone formation. Urol Res. 2005;33(5):383-9.

8. Williams Jr JC, Saw KC, Paterson RF, Hatt EK, Mcateer JA, Lingeman JE. Variability of renal stone fragility in shock wave lithotripsy. Urology. 2003;61(6):1092-6.

9. Ansari MS, Gupta NP, Seth A, Hemal AK, Dogra PN, Singh TP. Stone fragility: its therapeutic implications in shock wave lithotripsy of upper urinary tract stones. Int Urol Nephrol. 2003;35(3):387-92.

10. Richard S, Siewerdsen JH, Jaffray DA, Moseley DJ, Bakhtiar B. Generalized DQE analysis of radiographic and dual-energy imaging using flat-panel detectors. Med Phys. 2005;32(5):1397-413.

11. Brody WR, Butt G, Hall A, Macovski A. A method for selective tissue and bone visualization using dual energy scanned projection radiography. Med Phys. 1981;8(3):353-7.

12. Coursey CA, Nelson RC, Boll DT, et al. Dual-energy multidetector CT: how does it work, what can it tell us, and when can we use it in abdominopelvic imaging? Radiographics. 2010;30(4):1037-55.

13. Demirel A, Suma S. The efficacy of non-contrast helical computed tomography in the prediction of urinary stone composition in vivo. J Int Med Res. 2003;31(1):1-5.

14. Mostafavi MR, Ernst RD, Saltzman B. Accurate determination of chemical composition of urinary calculi by spiral computerized tomography. J Urol. 1998;159(3):673-5.

15. Mitcheson HD, Zamenhof RG, Bankoff MS, Prien EL. Determination of the chemical composition of urinary calculi by computerized tomography. J Urol. 1983;130(4):814-9.

16. Hillman BJ, Drach GW, Tracey P, Gaines JA. Computed tomographic analysis of renal calculi. AJR Am J Roentgenol. 1984;142(3):549-52.

17. Hidas G, Eliahou R, Duvdevani M, et al. Determination of renal stone composition with dual-energy CT: in vivo analysis and comparison with x-ray diffraction. Radiology. 2010;257(2):394-401.

18. Thomas C, Patschan O, Ketelsen D, et al. Dual-energy CT for the characterization of urinary calculi: In vitro and in vivo evaluation of a low-dose scanning protocol. Eur Radiol. 2009;19(6):1553-9.

19. Thomas C, Heuschmid M, Schilling D, et al. Urinary calculi composed of uric acid, cystine, and mineral salts: differentiation with dual-energy CT at a radiation dose comparable to that of intravenous pyelography. Radiology. 2010;257(2):402-9.

20. Graser A, Johnson TRC, Bader M, et al. Dual energy CT characterization of urinary calculi: initial in vitro and clinical experience. Invest Radiol. 2008;43(2):112-9.

21. Boll DT, Patil NA, Paulson EK, et al. Renal stone assessment with dual-energy multidetector CT and advanced postprocessing techniques: improved characterization of renal stone composition--pilot study. Radiology. 2009;250(3):813-20.

22. Primak AN, Fletcher JG, Vrtiska TJ, et al. Noninvasive differentiation of uric acid versus non-uric acid kidney stones using dual-energy CT. Acad Radiol. 2007;14(12):1441-7.

23. Saw KC, McAteer JA, Monga AG, Chua GT, Lingeman JE, Williams JC. Helical CT of urinary calculi: effect of stone composition, stone size, and scan collimation. AJR Am J Roentgenol. 2000;175(2):329-32.

24. Gupta NP, Ansari MS, Kesarvani P, Kapoor A, Mukhopadhyay S. Role of computed tomography with no contrast medium enhancement in predicting the outcome of extracorporeal shock wave lithotripsy for urinary calculi. BJU Int. 2005;95(9):1285-8.

25. Joseph P, Mandal AK, Singh SK, Mandal P, Sankhwar SN, Sharma SK. Computerized tomography attenuation value of renal calculus: can it predict successful fragmentation of the calculus by extracorporeal shock wave lithotripsy? A preliminary study. J Urol. 2002;167(5):1968-71.

26. Motley G, Dalrymple N, Keesling C, Fischer J, Harmon W. Hounsfield unit density in the determination of urinary stone composition. Urology. 2001;58(2):170-3.

27. Zarse CA, Hameed TA, Jackson ME, et al. CT visible internal stone structure, but not Hounsfield unit value, of calcium oxalate monohydrate (COM) calculi predicts lithotripsy fragility in vitro. Urol Res. 2007;35(4):201-6.

28. Saw KC, McAteer JA, Monga AG, Chua GT, Lingeman JE, Williams JC, Jr. Helical CT of urinary calculi: effect of stone composition, stone size, and scan collimation. AJR Am J Roentgenol. 2000;175(2):329-32.

29. Kijvikai K, de la Rosette JJ. Assessment of stone composition in the management of urinary stones. Nat Rev Urol. 2011;8(2):81-5.

30. Weissman M, Klein B, Berkowitz J. Clinical applications of infrared spectroscopy: Analysis of renal tract calculi. Analytical Chemistry. 1959;31(8):1334-8.

31. Chen WC, Wu SY, Liu HP, et al. Identification of melamine/cyanuric acid-containing nephrolithiasis by infrared spectroscopy. J Clin Lab Anal. 2010;24(2):92-9.

32. Schubert G. Stone analysis. Urol Res. 2006;34(2):146-50.

33. Gulley-Stahl HJ, Haas JA, Schmidt KA, Evan AP, Sommer AJ. Attenuated total internal reflection Fourier transform infrared spectroscopy: a quantitative approach for kidney stone analysis. Appl Spectrosc. 2009;63(7):759-66.

34. Davidson MT, Batchelar DL, Velupillai S, Denstedt JD, Cunningham IA. Analysis of urinary stone components by x-ray coherent scatter: characterizing composition beyond laboratory x-ray diffractometry. Phys Med Biol. 2005;50(16):3773-86.

35. Prien EL, Frondel C. Studies in urolithiasis; the composition of urinary calculi. J Urol. 1947;57(6):949-94.

36. Prien EL, Prien EL, Jr. Composition and structure of urinary stone. Am J Med. United States1968; p. 654-72.

37. Williams JC, Jr., Saw KC, Paterson RF, Hatt EK, McAteer JA, Lingeman JE. Variability of renal stone fragility in shock wave lithotripsy. Urology. United States2003; p. 1092-6; discussion 7.

38. Turgut M, Unal I, Berber A, Demir TA, Mutlu F, Aydar Y. The concentration of Zn, Mg and Mn in calcium oxalate monohydrate stones appears to interfere with their fragility in ESWL therapy. Urol Res. 2008;36(1):31-8.

39. Adams LG, Williams JC, McAteer JA, Hatt EK, Lingeman JE, Osborne CA. In vitro evaluation of canine and feline calcium oxalate urolith fragility via shock wave lithotripsy. Am J Vet Res. 2005;66(9):1651-4.

40. Mandhani A, Raghavendran M, Srivastava A, et al. Prediction of fragility of urinary calculi by dual X-ray absorptiometry. J Urol. 2003;170(4 Pt 1):1097-100.

41. Wang M, Shi Q, Wang X, Yang K, Yang R. Prediction of outcome of extracorporeal shock wave lithotripsy in the management of ureteric calculi. Urol Res. 2011;39(1):51-7.

Chapter 4 - Conclusions

The first objective of this work was to address the controversy in the published literature and determine whether there is good reason to expect sufficient signal difference in the dual energy measurements to differentiate between all stone materials with dual energy CT. The figure of merit for dual energy number showed greater ability to differentiate between stone materials than dual energy ratio at an acceptable voxel size and patient dose. Dual energy number was able to differentiate between all clinically relevant stone materials. Dual energy ratio was less effective at differentiating stone materials as it could not differentiate between magnesium ammonia phosphate and cystine, or calcium oxalate monohydrate and calcium oxalate dihydrate. The need to discriminate stone materials in vivo is to guide selection of the most appropriate treatment options and reduce patient morbidity. Based on the reported fragility of stones cystine and brushite are not amenable to shock wave lithotripsy so differentiating these from the other stone materials in vivo would enable appropriate treatment selection.(1-4) Additionally, struvite, uric acid and calcium oxalate dihydrate stones tend to fragment into small pieces while calcium oxalate monohydrate tends to fragment into larger pieces that are less likely to pass through the ureter or urethra.(5) Dual energy ratio does not have sufficient signal to noise ratio to provide clinically important information and discriminate calcium oxalate monohydrate, calcium oxalate dihydrate and cystine from other materials in a theoretical pure composition model. Therefore, is unlikely to be a useful measure in a clinically setting. However, dual energy number can differentiate all stone materials in a theoretical pure stone model.

Based on the theoretical model dual energy number should be able to differentiate between all stone materials in the Chapter 3 experiment but this did not hold true. The mean dual energy values for uric acid and cystine stones were comparable to the theoretical values from Chapter 2 but there was greater variability in the experimental and theoretical values for magnesium ammonium phosphate, calcium oxalate, and

brushite stones. The most likely explanation for the greater agreement in uric acid and cystine stones is that they were closer to a pure composition. Pure stones are uncommon in clinical practice and previous studies have had varied criteria for defining a pure stone and most range from 70-80% of a single stone material. This variation in purity is likely a major contributing factor to the varied results in the in vivo clinical determination of stone material. It is possible that even though dual energy number can theoretically discriminate between pure stone materials the inherent variation in stone purity noted clinically cannot be overcome with dual energy imaging. Other potential reasons for the variability in the DECT results could include errors in the CT measurements due to beam hardening artifact, partial volume averaging, misregistration of the dual energy images (due to patient motion between images), and CT scanner calibration errors. Partial volume averaging should not affect dual energy calculations as both the high and low energy measurements will be affected in a similar manner.(6) However, in small stones partial volume averaging may result in incorrect material characterization even with dual energy imaging because of inaccurate measurement of stone density.

Task specific beam filtration has been shown to improve material discrimination but only two previous studies evaluated the use of beam filtration for discrimination of urinary stones.(7, 8) The next objective of this work was to determine the optimal task specific beam filtration for differentiation of stone materials and whether the use of optimized task specific filter materials would substantially improve the differentiation of stone materials. Although range of materials and thicknesses were considered optimal a tin high energy filter and an erbium/tin low/high energy filter combination were evaluated further as they fell in the optimal parameters and were practical filter materials for clinical application. The optimal filter combination did result in an approximately four-fold increase in the figure of merit. Although this improvement was not needed to discriminate stones in the theoretical model this improvement could prove valuable in the clinical situation where stone purity and partial volume averaging may confound stone material discrimination.

It is important to remember the reason for requiring an in vivo determination of stone material is to determine the best treatment option for the patient to increase treatment

success and decrease patient morbidity. This means identifying stones that are likely to be successfully fragmented with ESWL versus those that are unlikely to be fragmented and will require surgical intervention. Determining stone composition is not the only factor in the assessment of stone fragility for ESWL as it has also been shown that within a specific chemical composition (particularly calcium oxalate stones) there is great variability in stone fragility (co-efficient of variability 60%).(9) Within calcium oxalate stones the concentration of magnesium, manganese and zinc were significantly lower in stones that were successfully fragmented with ESWL versus those that failed treatment.(5) Adams et. al. compared the fragility of calcium monohydrate stones from dogs and cats and found that feline stones were harder to break than canine stones in spite of the same chemical composition.(10) This may be due to varying amounts of organic material or a mix of minerals being present.(9) Mandhani et. al. used dual x-ray absorptiometry (DXA) to assess stone fragility and determined that fragility was correlated to stone mineral content and not mineral density. They hypothesized that a classification scheme that is independent of composition and based on stone mineral content would answer the clinically relevant question of whether stones can be fragmented with ESWL or not.(11) Therefore, given all the challenges with using dual energy CT to determine the composition of urinary stones, including the difficultly in adding task specific beam filtration to the CT scanner, future studies should focus on the more clinically relevant question of whether dual energy CT can adequately differentiate between fragile and non-fragile stones.

References:

1. Evan AP, Coe FL, Lingeman JE, Worcester E. Insights on the pathology of kidney stone formation. Urol Res. 2005;33(5):383-9.

2. Gupta NP, Ansari MS, Kesarvani P, Kapoor A, Mukhopadhyay S. Role of computed tomography with no contrast medium enhancement in predicting the outcome of extracorporeal shock wave lithotripsy for urinary calculi. BJU Int. 2005;95(9):1285-8.

3. Joseph P, Mandal AK, Singh SK, Mandal P, Sankhwar SN, Sharma SK. Computerized tomography attenuation value of renal calculus: can it predict successful fragmentation of the calculus by extracorporeal shock wave lithotripsy? A preliminary study. J Urol. 2002;167(5):1968-71.

4. Williams Jr JC, Saw KC, Paterson RF, Hatt EK, Mcateer JA, Lingeman JE. Variability of renal stone fragility in shock wave lithotripsy. Urology. 2003;61(6):1092-6.

5. Turgut M, Unal I, Berber A, Demir TA, Mutlu F, Aydar Y. The concentration of Zn, Mg and Mn in calcium oxalate monohydrate stones appears to interfere with their fragility in ESWL therapy. Urol Res. 2008;36(1):31-8.

6. Primak AN, Fletcher JG, Vrtiska TJ, et al. Noninvasive differentiation of uric acid versus non-uric acid kidney stones using dual-energy CT. Acad Radiol. 2007;14(12):1441-7.

7. Primak AN, Ramirez Giraldo JC, Liu X, Yu L, McCollough CH. Improved dual-energy material discrimination for dual-source CT by means of additional spectral filtration. Med Phys. 2009;36(4):1359-69.

8. Qu M, Ramirez-Giraldo JC, Leng S, et al. Dual-energy dual-source CT with additional spectral filtration can improve the differentiation of non-uric acid renal stones: an ex vivo phantom study. AJR Am J Roentgenol. 2011;196(6):1279-87.

9. Williams JC, Jr., Saw KC, Paterson RF, Hatt EK, McAteer JA, Lingeman JE. Variability of renal stone fragility in shock wave lithotripsy. Urology. United States2003; p. 1092-6; discussion 7.

10. Adams LG, Williams JC, McAteer JA, Hatt EK, Lingeman JE, Osborne CA. In vitro evaluation of canine and feline calcium oxalate urolith fragility via shock wave lithotripsy. Am J Vet Res. 2005;66(9):1651-4.

11. Mandhani A, Raghavendran M, Srivastava A, et al. Prediction of fragility of urinary calculi by dual X-ray absorptiometry. J Urol. 2003;170(4 Pt 1):1097-100.

Appendices

Appendix A: Imaging parameters used in previously reported dual energy computed tomography evaluations

Parameters	CT scanner	Energy setting - high	Energy setting - low	mAs high : mAs low	Collimation (mm)	Method	Medium	Stone analysis
Mitcheson et al.	Siemens Somaton-2	125kV 460mA	77 kV 747 mA	1.6	2	in vitro	water	-
Mostafavi et al.	GE Hi-Speed	120 kV 240 mA	80 kV 240 mA	1	1	in vitro	air	X-ray crystallography polarized microscopy 100% pure
Bellin et al.	Siemens Somatom Plus 4	140 kV 200 mAs	80 kV 200 mAs	1	3	in vitro	pig kidney	Crystallography stereomicroscopy classified by predominant component
Thomas et al. (Radiographics)	Seimans DE CT	140 kV 23 maS	80 kV 105 mAs	4.6	5	in vitro	-	IR spectroscopy
Thomas et al. (Eur Radiol)	Siemens Somotron Definition	140 kV 46 mAs	80 kV 210 mAs	4.6	1	in vitro	-	IR spectroscopy
Graser et al.	Siemens Care dose 4D	140 kV 76 mAs	80 kV 342 mAs	4.5	2	in vivo	50 x 20 cm water	-
Graser et al.	Siemens Care dose 4D	140 kV 76 mAs	80 kV 342 mAs	4.5	2	in vitro	-	chemical analysis
Boll et al.	Siemens Somatom Definition	140 kV 118 mAs	80 kV 499 mAs	1	1	in vivo	water 15 cm	IR spectroscopy >97% pure
Matlaga et al.	Siemens Somatom Definition	140 kV 110 mAs	80 kV 486 mAs	1.5	1.5	in vivo	water 21 cm	chemical reaction IR microscopy

Appendix B: Reported CT attenuation values of stones after exposure using a high energy (120-140kV) setting

	Calcium oxalate	COM	COD	Struvite	Cystine	Uric Acid	Brushite	Apatite	Calcium containing
Mitcheson et al.	>1023			651 +/- 108	703 +/- 69	540 +/- 107	>1023		
Mostafavi et al.	1620 +/- 232	1645 +/- 238	1417 +/- 234	666 +/- 87	711 +/228	409 +/- 118 *	1703 +/- 161		
Bellin et al.		1203 +/- 195	631 +/- 113	510 +/- 135	482 +/- 97	377 +/- 142		703 +/- 183	
Thomas et al. (Eur Radiol)		795 +/- 180	844 +/- 173			439 +/- 70			
Graser et al.					797 +/- 50	371 +/- 25			1322 +/- 206
Graser et al.					805	415 +/- 159			1122 +/- 429
Boll et al.				1077-1100	513-747	443-615			346-1939
Matlaga et al.	1091.6 +/- 364.8					347.0 +/- 56.4	722.2 +/- 248.5		

* indicates significant differences were noted between these stones

Appendix C: Reported CT acquired dual energy ratio values of stones (HU high energy beam/HU low energy beam)

	Calcium oxalate	**COM**	**COD**	**Struvite**	**Cystine**	**Uric Acid**	**Brushite**	**Apatite**
Thomas et al. (Radiographics)		1.5 (1.42-1.77)	1.5	1.34	1.36 (1.27-1.39)*	1.06 (0.88-1.18)*	1.53 (1.46-1.57)	1.49 (1.44-1.53)
Thomas et al. (Eur Radiol)		1.19 +/- 0.05	1.21 +/- 0.03			1.0.1 +/- 0.04		
Matlaga et al.	1.44*					1.04*	1.51*	

* indicates significant differences were noted between these stones

Appendix D: Reported CT acquired dual energy attenuation values of stones (HU low energy beam – HU high energy beam)

	Calcium oxalate	COM	COD	Struvite	Cystine	Uric Acid	Brushite
Mostafavi et al.	-	691 +/- 109*	412 +/- 86*	131 +/- 65*	332 +/- 65*	0 +/- 41*	602 +/- 50*
Matlaga et al.	270.7					11.45*	369.5

* indicates significant differences were noted between these stone

Appendix E: Estimation of average linear attenuation coefficient of stone material

The average linear attenuation coefficient of a material determines the attenuation of an x-ray beam and can be calculated using

$$N = N_0 e^{-\left(\frac{\mu}{\rho}\right)\rho x} \tag{E.1}$$

where N is the number of photons incident on the detector with the stone in the path, N_0 is the number of photons without the stone material, μ [cm^{-1}] is the average linear attenuation coefficient of the material, ρ [g/cm^3], is the density of the material and *x* [cm] is the thickness of the material. Therefore

$$\ln\left(\frac{N}{N_0}\right) = -\frac{\mu}{p} px$$
$$\mu = \frac{1}{x}\ln\left(\frac{N_0}{N}\right) \tag{E.2}$$

Appendix F: Theoretical derivation of noise in the CT image

With reference to Figure 2-1 Faulkner and Moores (1) have shown that noise in linear attenuation coefficient (μ) for each pixel obtained using filtered back-projection reconstruction assuming a mono-energetic x-ray beam is given by [cm^{-1}]:

$$\sigma_\mu^2 = \frac{\pi^2}{12 N_\theta w^2}\sigma_p^2 \tag{F.1}$$

where N_θ is the number of angular increments, w is the width of the detector [cm], and σ_p^2 is the variance in log-projection values p as determined from a single detector element from one projection along the central ray.

Monoenergetic model

If the number of photons interacting with the detector without a phantom present is $d_0 = kN_0E\varepsilon$ and the number of photons interacting with the detector with a phantom present is $d = kNE\varepsilon$ where k is a constant of proportionality relating detector signal to absorbed energy and it is assumed all x-ray energy is absorbed in each x-ray interaction, E is the energy of the interacting photon, and ε is the detector quantum efficiency.

Therefore, the projection measurement for a monoenergetic beam of x-rays is given by

$$p = \ln\frac{d_0}{d} = \ln\left(\frac{kN_0E\varepsilon}{kNE\varepsilon}\right). \tag{F.2}$$

The log-projection variance is given by

$$\begin{aligned}\sigma_p^2 &= \frac{1}{d^2}\sigma_d^2 \\ &= \frac{1}{k^2N^2E^2\varepsilon^2}\cdot\frac{1}{N\varepsilon} \\ &= \frac{1}{N\varepsilon}\end{aligned} \tag{F.3}$$

where N is the number of x-ray photons incident on one detector element in one projection and is given by

$$N = \frac{Q_0 I w s N_d e^{-\mu L}}{N_\theta N_p} \tag{F.4}$$

and where Q_0 is the number of photons per cm^2 per mAs incident on the detector without the phantom [$cm^{-2}mAs^{-1}$], I is the mAs value for the slice, *w* the detector width [cm], *s* the slice thickness [cm], N_d the number of detector elements irradiated by the beam, N_θ the number of angular increments, N_p the number of projections, and ε is the detector quantum efficiency. In our work the number of projections is equal to the number of detector elements irradiated by the beam. Therefore,

$$\sigma_\mu^2 = \frac{\pi}{12 w^2 e^{-\mu L} [Q_0 I w s] \varepsilon} \tag{F.5}$$

where the term in square brackets gives the average number of quanta incident on one detector element along the central ray without the phantom for the entire slice scan (L is the phantom diameter).Noise in a CT image is therefore given by σ_H^2 from equation (2.2) giving

$$\begin{aligned} \sigma_H^2 &= \left| \frac{10^3}{\mu_w} \right|^2 \sigma_\mu^2 \\ &= \frac{10^6 \pi^2}{12 w^3 s} \frac{1}{Q_0 I \mu_w^2 e^{-\mu L} \varepsilon} \end{aligned} \tag{F.6}$$

This simple model has been effective is developing an understanding of noise in CT images for filtered back projection reconstruction using a ramp filter (Shepp-Logan) for ideal detector elements. (1)

Polyenergetic Model

We extend the monoenergetic model to include a broad spectrum of x-ray energies for dual energy imaging. The log-projection is then given by the ratio of two measurements:

$$p = \frac{kws\int Q_0(E)E\varepsilon(E)dE}{kws\int Q(E)E\varepsilon(E)dE} \tag{F.7}$$

where Q(E) and $Q_0(E)$ [cm^{-2} keV^{-1} mAs^{-1}] describe the spectra incident on a single detector element with and without a phantom. The variance in p is addressed by noting that each energy in a discrete spectral representation is independent. Thus if $d = d_1+d_2+\ldots$ then

$$\begin{aligned}
\sigma_p^2 &= \left|\frac{dp}{dd}\right|^2 \sigma_d^2 \\
&= \left|\frac{dp}{dd_1}\right|^2 \sigma_{d_1}^2 + \left|\frac{dp}{dd_2}\right|^2 \sigma_{d_2}^2 + \ldots \\
&= \frac{1}{d^2}\left[\left|\frac{dd}{dd_1}\right|^2 \sigma_{d_1}^2 + \left|\frac{dd}{dd_2}\right|^2 \sigma_{d_2}^2 + \ldots\right] \\
&= \frac{1}{d^2}\left[\sigma_{d_1}^2 + \sigma_{d_2}^2 + \ldots\right]
\end{aligned} \tag{F.8}$$

Where the detector signal and variance in the *i*th energy bin is given by:

$$d_i = \frac{kwsQ(E_i)IE_i\varepsilon(E_i)\Delta E}{N_\theta N_p} \tag{F.9}$$

and

$$\sigma_{d_i}^2 = \frac{k^2wsQ(E_i){E_i}^2\varepsilon(E_i)\Delta E}{N_\theta N_p} \tag{F.10}$$

Generalizing to the limit of infinitesimal energy bins gives

$$d = \frac{kws\int Q(E)IE\varepsilon(E)dE}{N_\theta N_p} \tag{F.11}$$

and

$$\sigma_d^2 = \frac{k^2 ws \int Q(E) I E^2 \varepsilon(E) dE}{N_\theta N_p} \quad . \tag{F.12}$$

Substituting (F.11) and (F.12) into equation (F.8) gives

$$\sigma_p^2 = \frac{N_\theta \int Q_0(E) I E^2 \varepsilon(E) dE}{ws \left| \int Q(E) I E \varepsilon(E) dE \right|^2} \quad . \tag{F.13}$$

Therefore from equation (F.1)

$$\sigma_\mu^2 = \frac{\pi^2}{12 w^2 ws} \frac{\int Q_0(E) I \varepsilon(E) E^2 \, dE}{\left[\int Q(E) I \varepsilon(E) E \, dE \right]^2} \quad . \tag{F.14}$$

and from equation (F.6)

$$\sigma_H^2 = \frac{10^6 \pi^2}{12 w^2 ws \mu_w^2} \frac{\int_0^{kV} Q_0(E) I E^2 \varepsilon(E) dE}{\left[\int_0^{kV} Q(E) I E \ \varepsilon(E) dE \right]^2} \tag{F.15}$$

which can be compared with equation (F.6) to show the impact of the spectral shape on CT image noise.

Appendix G: Table of variables

Variable	Definition	Unit
Q_0	Normalized density of photons incident on the detector along the central ray of each CT projection measurement when no phantom is present	$cm^{-2}mAs^{-1}$
μ	Linear attenuation coefficient	cm^{-1}
I	Product of the tube current and exposure time for a 360° rotation	mAs
N_p	Number of projections or ray sums in the set of projections at one angular position	
N_d	Number of detector elements subtended by the phantom	
N_θ	Number of angular increments	
s	Slice thickness	cm
w	Detector width	cm
L	Phantom diameter	cm
ε	Detector quantum efficiency	
T_f	Transmission of a filter added to the beam near the source	
K_{CT}	Air KERMA at isocenter in the absence of a phantom	mGy
R_K	Ratio of air KERMA at a given location in a phantom to air K_{CT}	

Appendix H: List of abbreviations

COM	Calcium oxalate monohydrate
COD	Calcium oxalate dihydrate
MAP	Magnesium ammonium phosphate
CAP	Carbonate apatite
HAP	Hydroxyl apatite
BRU	Brushite (calcium hydrogen phosphate dihydrate)
UA	Uric acid
CYS	Cystine
ESWL	Extracorporeal shock wave lithotripsy
PCNL	Percutaneous nephrolithotomy
FTIR	Fourier transform infrared spectroscopy
ATR-FTIR	Attenuated total internal reflection Fourier transform infrared spectroscopy
CSCT	Coherent scatter computed tomography
DECT	Dual energy computed tomography

Curriculum Vitae

Name: Stephanie Nykamp

Post-secondary Education and Degrees:
University of Guelph
Guelph, Ontario, Canada
1993-1997 DVM

Honours and Awards:
K.M. Bhatnager Memorial Humanitarian Award (2014)
Carl J. Norden Distinguished Teaching Award (2011)

Related Work Experience
Associate Dean Clinical Program
University of Guelph
2013-present

Associate Professor (tenured)
University of Guelph
2010-present

Assistant Professor
University of Guelph
2003-2010

Selected Publications:

1. Bourzac CA, Koenig JB, Link KA, Nykamp SG, Koch TG. Comparative labeling of equine umbilical cord blood-derivced and bone marrow-derived mesenchymal stromal cells and Molday ION Rhodamine B for ex vivo cell tracking with MRI. *Am J Vet Res*. Accepted June 2014.
2. Huska J, Gaitero L, Brisson B, Nykamp S, Thomason J, Sears W. Comparison of the access window created by hemilaminectomy and mini-hemilaminectomy in the thoracolumbar spinal canal using computed tomography. Can Vet J. 2014;55(5):499-455.
3. Oblak M, Boston S, Woods J, Nykamp S. Comparison of concurrent imaging modalities in staging of dogs with appendicular osteosarcoma. *Vet Comparative Onco*. 2013 ePub
4. Gaitero L, Nykamp S, Daniel G, Monteith G. Comparison between cranial thoracic intervertebral disc herniations in German Shepherd Dogs and other large breed dogs. *Vet Radiol Ultrasound*. 2013 54(2) 113-138.
5. Mitchell CW, Nykamp SG*, Foster R, Cruz R, Monteith G. The use of magnetic resonance imaging in evaluating horses with spinal ataxia. *Vet Radiol Ultrasound*. 2012 53(6) 613-620.

6. Webb JA, Nykamp SG, Gauthier MJ, Kirby GM. Ultrasonographic and laboratory screening in healthy mature golden retriever dogs. *Canadian Veterinary Journal.* 2012 52(6) 626-630.
7. Chalmers HJ, Nykamp SG, Lerer A. The Ontario Veterinary College hip and elbow certification program – assessing inter and intra-observer repeatability and comparison of findings to the Orthopedic Foundation for Animals. *Can Vet J*. 2013 54 42-46
8. Bergeron LH, Nykamp SG, Brisson BA, Madan P, Gartley CJ. An evaluation of the efficacy of B-mode and color Doppler ultrasonography of canine ovaries for detecting the preovulatory LH peak. *Theriogenology*. 2012 epub.
9. Reynolds D, Brisson BA, Nykamp SG. Agreement between magnetic resonance imaging, myelography and surgery for detecting recurrent naturally occurring Type I thoracolumbar intervertebral disc disease in dogs. *VCOT*. 2012 epub.
10. Black B, Cribb CN, Nykamp S, Thomason JJ, Trout DR. Effect of local anesthetic deposition into structures of the equine foot on subsequent magnetic resonance imaging. *Eq Vet J.* 2012 epub.
11. Squires Bos A, Brisson BA, Nykamp SG, Poma R, Foster RA. Accuracy, intermethod agreement and inter-reviewer agreement for use of magnetic resonance imaging and myelography in small-breed dogs with naturally-occurring first time intervertebral disk extrusion. *J Am Vet Med Assoc*. 2012 240(8):969-977.
12. Singh AM, Brisson B, O'Sullivan L, Solomon J, Nykamp SG, Thomason J. Percutaneous catheterization an embolization of the thoracic duct in dogs: A feasibility study. *Am J Vet Research*. 2011 72(11):1527-1534.
13. Singh A, Brisson BB, Nykamp S, O'Sullivan ML. Comparison of computed tomographic and radiographic popliteal lymphadenography in normal dogs. Vet Surg. 2011 40(6) 762-767.
14. Hayes G, Mathews K, Doig, Kruth S, Boston S, Nykamp S, Poljak Z Dewey C. The feline acute patient physiologic and laboratory evaluation (feline APPLE) score: A severity illness stratification system for hospitalized cats. *J Vet Intern Med*. 2011 25(1) 26-28.